JOURNAL OF Applied Polymer SCIENCE

Use of poly(3-hydroxybutyrate)/niobium oxyhydroxide nanocomposites in photocatalysis: Effect of preparation methods

Ana Pacheli Heitmann Rodrigues,[1] Italo Coura Rocha,[2] Arthur Caron Mottin,[3] Luiz Carlos Alves Oliveira,[1] Patrícia Santiago de Oliveira Patrício [2]

[1]Department of Chemistry, Universidade Federal de Minas Gerais, Av. Antônio Carlos 6627, Campus Pampulha, MG 31270-901, Brazil

[2]Department of Chemistry, Centro Federal de Educação Tecnológica de Minas Gerais, CEFET-MG, Av. Amazonas 5253, Nova Suiça, MG 30421-169, Brazil

[3]School of Mining Engineering, Thematic Network in Materials Engineering-REDEMAT, R. nove 293, Ouro Preto, MG 35400-000, Brazil

Correspondence to: P. S. O. Patrício (E-mail: patriciapatricio@des.cefetmg.br)

ABSTRACT: In this work, nanocomposites were obtained by the dispersion of niobium oxyhydroxide into a poly(3-hydroxybutyrate) (PHB) matrix by different preparative methods. These methods led to changes in the polymer morphology and in their photocatalytic properties. Thermal and structural properties of the nanocomposites were investigated using thermogravimetric analysis (TGA), differential scanning calorimetry (DSC), and Fourier transform infrared spectroscopy (FTIR)–attenuated total reflection (ATR). Scanning electron microscopy images were analyzed in order to observe the different morphologies of nanocomposites as well as the distribution of niobium nanoparticles in the PHB matrix. The chemical interactions between the polymer and niobium nanoparticles were observed in the FTIR–ATR and thermal analyses. The results of TGA and DSC indicated an improvement in the thermal stability of the polymer and the action of inorganic nanoparticles as nucleating agents in the process of heterogeneous nucleation of PHB. The composites exhibited good catalytic activity for the removal of methylene blue dye from an aqueous medium (~90%) during a photocatalytic process. The different morphologies of PHB/niobium oxyhydroxide composites directly influenced the catalytic activity of the material due to the difference in the dispersion of nanoparticles. © 2017 Wiley Periodicals, Inc. J. Appl. Polym. Sci. **2018**, *135*, 45836.

KEYWORDS: biodegradable; catalysts; differential scanning calorimetry; thermoplastics

Received 8 May 2017; accepted 7 September 2017
DOI: 10.1002/app.45836

INTRODUCTION

The development of nanocomposites with biodegradable polymers produced from renewable sources has received considerable attention in recent years. Materials with this feature are attractive, as they can be assimilated and decomposed by microorganisms, being easily converted via enzymatic routes into simple and mineralized compounds.[1] Among the polymers that have been studied, poly(3-hydroxybutyrate) (PHB) stands out as a bio-polyester with properties comparable to those of polymers such as polypropylene and barrier properties analogous to those of poly(ethylene terephthalate), and poly(vinyl chloride).[2] However, limitations such as high brittleness and rigidity are responsible for low mechanical performance, hindering the development of practical applications of PHB.[3–5] The polymer shows a structure characterized by large spherulites formed during cooling in the molten state which are responsible for its brittleness. Furthermore, its thermal degradation occurs at approximately 200 °C, which is near its melting temperature (180 °C), indicating that processing in extruders or by injection molding must occur at limited temperatures.[6]

To overcome these drawbacks, chemical modification in the polymer chains is an approach to improve the mechanical properties of PHB and consequently increase its applicability. The resulting improvements in the processing performance and physical properties can enable the development of new materials.[7] The most frequent ways are: (1) method of chemical modification as the synthesis of co-monomers of poly(hydroxyalkanoates); (2) incorporation of additives such as plasticizers and inorganic fillers as nucleating agents, and (3) formulation of composites and blends. For industrial applications, blends and composites whose preparation does not involve synthetic steps are desirable materials because they are easy to obtain and are cost-effective.[8]

© 2017 Wiley Periodicals, Inc.

10974628, 2018, 7, Downloaded from https://onlinelibrary.wiley.com/doi/10.1002/app.45836 by INPI - Instituto Nacional da Propriedade Industrial, Wiley Online Library on [18/06/2023]. See the Terms and Conditions (https://onlinelibrary.wiley.com/terms-and-conditions) on Wiley Online Library for rules of use; OA articles are governed by the applicable Creative Commons License

The physical, mechanical, and thermodynamic properties of semi-crystalline polymers are strongly influenced by the polymers' morphology. The morphology is related to the chemistry and is a result of the arrangement of the polymer chains and the applied deforming forces.[9,10] The polymer chains are organized into different crystal structures depending on the applied processing mode. PHB, like other thermoplastics, can be processed by injection molding, extrusion and casting. Additionally, other processing modes are applied in the development of different morphologies for such polymers and to obtain microspheres (MS), casting, and nanofibers (NF), thus increasing the attractiveness of PHB. The electrospinning process allows the production of continuous fibers with a diameter of a few nanometers. The surface structures of these materials promote potential application in medical and industrial areas.[11] An electrostatic field is applied to a solution of the polymer, forming a jet of fiber that travels through the atmosphere and allows the solvent to evaporate; resulting in the solid deposition of the polymer fibers at the collector in the form of nonwoven webs.[12] Thermoplastic compression molding was used as an attempt to improve PHB properties through the application of stress including the use of rotors with different processing conditions for mixing.[13] The main steps in this process involve the melting of the polymer at high temperatures; applying the pressure in the material by making it flow into the mold and cooling the material to a temperature at which the film can be removed from the mold without any deformation.[14] Nano- and microstructured polymer systems can act as a transport medium for various substances incorporated in the materials. Several techniques can be used to prepare polymeric microparticles. The choice of technique depends on the characteristics of the polymer and the intended use.[15] In the single emulsion (o/w), method employed in this work, the polymer solution is added to aqueous poly(vinyl alcohol) (PVA) solution used as a surfactant for MS production. The precipitation of the polymer is accelerated and the encapsulation of the substances can be compromised.[16] Another method to producing PHB films is to use the solvent casting process, which involves evaporating the solvent from the polymer solution.[17] Solvent casting allows the adaptation of the mechanical and optical properties of the film by varying processing parameters such as time and temperature of the solvent to obtain high quality films. The solvent casting process is capable of producing uniform and porous films that can degrade rapidly in specific conditions.[18] These methods are versatile for obtaining materials at the nano- or micro-scale with different porosities and surface areas. The literature reports the use of these materials as catalysts,[19] as scaffolds in tissue repair[20] and for controlled release of drugs.[21]

The use of PHB as a support for catalysts was first reported by Yew *et al.*,[22] who studied the polymer system PHB/TiO_2, but with a high content of the semiconductor (57 wt %) to degrade organic contaminants and improve antibacterial activity through photocatalytic sterilization. The results demonstrate significant photocatalytic removal (~96%). Sridewi *et al.*[23] determined the efficiency of photocatalysis of real industrial wastewater discolored with a high load of dyes using the nanocomposite PHB/TiO_2 (40 wt %) as the catalyst. Higher rates of removal (96%) were obtained after six cycles of reuse. Moreover, the efficiency was >80%. In addition, the toxicity of the aqueous medium was evaluated after the decolorization of the effluent, and it was found that no toxic intermediates were formed in the photocatalytic process. In 2011, the same group used a composite obtained by electrospinning the catalyst PHB/TiO_2 (50 wt %) for the removal of triphenylmethane from a dye class.[24] The adsorption and photocatalytic processes were used to simultaneously remove organic molecules. Discoloration reached ~100% in 45 min, but 78% was obtained by adsorption without the formation of toxic compounds in the environment.

In general, the catalysts most used in photocatalytic reactions are TiO_2 nanoparticles due to high catalytic activity, their chemical stability, and well-known mechanisms of photocatalysis.[25] Other inorganic oxides, as niobium oxide also are used in the photocatalysis process for the degradation of dyes. Although Nb_2O_5 has a similar band gap of TiO_2, it is possible to produce a material with a low band gap value by modifying the niobium. Thus, it is possible, for example, to treat the niobium catalyst with hydrogen peroxide, promoting the transformation of the Brönsted acid sites into oxidizing sites (peroxo sites) on its surface increasing the catalytic activity of the semiconductor.[26] Our research group works on the development of these catalysts due to the interest of our country, which is the main producer of niobium with 60% of the world production.[27] In the present work, we report the development of composites based on PHB polymer and niobium oxyhydroxide, with different shapes to be used as photocatalysts. The compounds were obtained by different methods of preparation, characterized and evaluated for their photocatalytic activity to remove methylene blue dye from aqueous media in the presence of ultraviolet (UV) light.

EXPERIMENTAL

Catalytic Syntheses: Niobium Oxyhydroxide (S_2)

For the synthesis of niobium oxyhydroxide, labeled S_2, 46.2 mmol of the precursor ammonium niobium oxalate salt ($NH_4[NbO(C_2O_4)_2(H_2O)](H2O)_n$), provided by CBMM (Rio de Janeiro, Brazil) was dissolved in 100 mL of distilled water at 90 °C. After complete dissolution of the salt, NH_4OH was added slowly to the solution until pH 7, for precipitation of the niobium oxyhydroxide. The suspension was kept under constant stirring for 12 h and the white solid was filtered, washed, and oven-dried. The obtained material was dispersed in distilled water and treated with 30% hydrogen peroxide. The synthesis was conducted via a previously reported procedure.[28–30]

Composite Preparation

Films by Casting. The films of PHB/S_2_2 were obtained by the casting technique. For the preparation of films, PHB powder (BIOCYCLE) was dissolved in chloroform and dimethylformamide at a ratio 1:5, to which niobium oxyhydroxide (S_2) was added at a concentration of 2 wt %. The solution was placed under constant agitation and heated at approximately 55 °C until complete dissolution over 4 h. The mixture was poured into glass Petri dishes, and the solvent was left to evaporate at room temperature for 72 h, after which the samples were put in the oven at 60 °C for 24 h.

MS. PHB and PHB/S2_2 MS were obtained, respectively, from an aqueous PVA (Sigma Aldrich) solution (3% v/v) and a solution of PHB in chloroform and dimethylformamide (1:5). The nanoparticles were dispersed in the catalyst PHB solution (2 wt %). The aqueous PVA solution was poured into the polymer solution under mechanical stirring and heated at 50 °C for 6 h. The obtained beads were filtered and dried at room temperature. The remaining PVA was manually separated from the MS.

NF. NF of PHB and PHB/S2_2 were obtained by electrospinning. The PHB powder (BIOCYCLE) was solubilized in chloroform and dimethylformamide at a ratio 1:5. In the preparation of NF, PHB/S2_2 was added to the catalyst (S2) at a concentration of 2 wt %. In the process of electrospinning, the solution was ejected from the tip of the needle ($D = 2$ mm) to generate positively charged ultrafine fibers on the static collector. The parameters for the production of NF were distance of 10 cm from the needle to the collector, injection rate of 12 mm/h, and potential difference equal to 14.0 kV. All tests were conducted at room temperature.

Films by Melt Processing. The pure PHB and the mixture of PHB and S_2 catalyst (2 wt %) were added to a Thermo Haake (Polydrive mixer) mixing chamber at a temperature of 175 °C for 5 min. After cooling, the obtained mixture was added to a knife mill (Mill KIE 600). Pressing was conducted in several steps at 180 °C for 3 min at 2 MPa, and the films were cooled at room temperature.

Characterization of Materials

The morphology of the developed composites was characterized by a scanning electron microscope (SEM) (JEOL, model 840A) operating at 7 kV. The films were coated with a 5 nm carbon layer using a BAL-TEC 010 MC instrument.

Fourier transform infrared (FTIR) spectroscopic data were obtained with a Shimadzu Prestige 21 spectrophotometer equipped with an attenuated total reflection accessory (ATR with Krs-5 crystal) in reflection mode. The spectra were collected in the range 4000–400 cm^{-1} with a scan number of 60 and resolution of 4 cm^{-1}.

Thermogravimetric analysis (TGA) curves were obtained under nitrogen atmosphere (50 mL/min) and heating rate of 10 °C/min from room temperature to 600 °C using the simultaneous TG/DTA thermogravimetric analyzer (Shimadzu, model DTG 60). The thermal properties were directly determined as DTG curves derived from the original TGA thermogram using the product software.

The DSC curves were obtained on a TA Instruments DSC2010 thermo analyzer. The samples were put into a hermetically sealed alumina pan. In the first run, the samples were heated in the temperature range from 30 to 185 °C, maintained at this temperature for 3 min, cooled to −30 °C and heated again to 190 °C at a rate of 10 °C min^{-1} under a dynamic nitrogen atmosphere (50 mL min^{-1}). The DSC curves shown are for the second run of heating. The crystallinity index (X_c) of PHB and the PHB/niobium oxyhydroxide composites was calculated from eq. (3):

$$X_c = \frac{\Delta H_n \times 100}{\Delta H_0 \times w(\mathrm{PHB})} \quad (1)$$

where ΔH_n is the melting enthalpy of the sample (J/g), a value of 146 J/g ΔH_0 was used as the heat of melt for 100% crystalline PHB, and w(PHB) is the weight fraction of the PHB sample.[31]

Catalytic Tests

The catalytic tests were performed at 25 °C using 15 mL of methylene blue solution (20 mg L^{-1}) as the model molecule. A 0.5 g aliquot of the polymer film was used, with stirring at 330 rpm using a magnetic stirrer for predetermined times of 10–120 min. A UV lamp was used (mercury vapor $\lambda = 254$ nm) with power of 15 W. The samples were positioned at 20 cm from UV light. The oxidation efficiency was monitored with a UV–vis spectrophotometer (Shimadzu UV-1601-PC) at wavelengths of 664 nm.

RESULTS AND DISCUSSION

Characterization of the Composites

The PHB/niobium oxyhydroxide (S_2) nanocomposites with 2 wt % of inorganic particles were prepared through different preparative methods, generating materials with different morphologies, which were labeled as NF, casting films (CS), MS, and thermo-processing films (PR).

The morphology of the materials was evaluated by SEM, and the images obtained are shown in Figure 1. Furthermore, EDS spectra of samples containing niobium oxyhydroxide are shown in Figure 1. In PHB and PHB/S_2_2 obtained by electrospinning (NF), SEM images show the presence of PHB NF entanglement. Beads can be observed in the pure PHB NF, and these are attributed to insolubilized polymer grains. This occurs due to certain complications during the electrospinning process.[32] However, the formation of PHB NF with a smooth and uniform surface and the absence of grains is also seen in PHB/S_2_2 NF. It is suggested that the addition of particles of niobium oxyhydroxide favored the process of formation of PHB NF. The presence of niobium oxyhydroxide was confirmed by the signal corresponding to niobium in the EDS spectrum. These spectra were collected focusing on the lighter regions (spheroidal—inside circle) highlighted in the image with a greater magnification in the top right-hand corner of the corresponding SEM image. Spheroidal regions of submicron sizes were not observed in the SEM images of the pure polymer. Thus, it is suggested that particles of niobium are well distributed along the polymer NF, but as clusters with size 1 μm approximately. In the pioneering work using TEM, it was revealed that the niobium oxyhydroxide (S_2) exists as nanoparticles.[19] However, it is suggested here that the light phases in the SEM images are agglomerates of nanoparticles present in the polymer matrix. In samples of all types, EDS spectra (not shown here) of pure PHB were obtained and peaks related to carbon and oxygen were observed.

SEM images of the samples PHB MS and PHB/S_2_2 MS show the presence of spheres of different sizes and micron dimensions. In the inset images with larger magnification, the formation of MS is observed, with a size of approximately 5 μm. The

10974628, 2018, 7, Downloaded from https://onlinelibrary.wiley.com/doi/10.1002/app.45836 by INPI - Instituto Nacional da Propriedade Industrial, Wiley Online Library on [18/06/2023]. See the Terms and Conditions (https://onlinelibrary.wiley.com/terms-and-conditions) on Wiley Online Library for rules of use; OA articles are governed by the applicable Creative Commons License

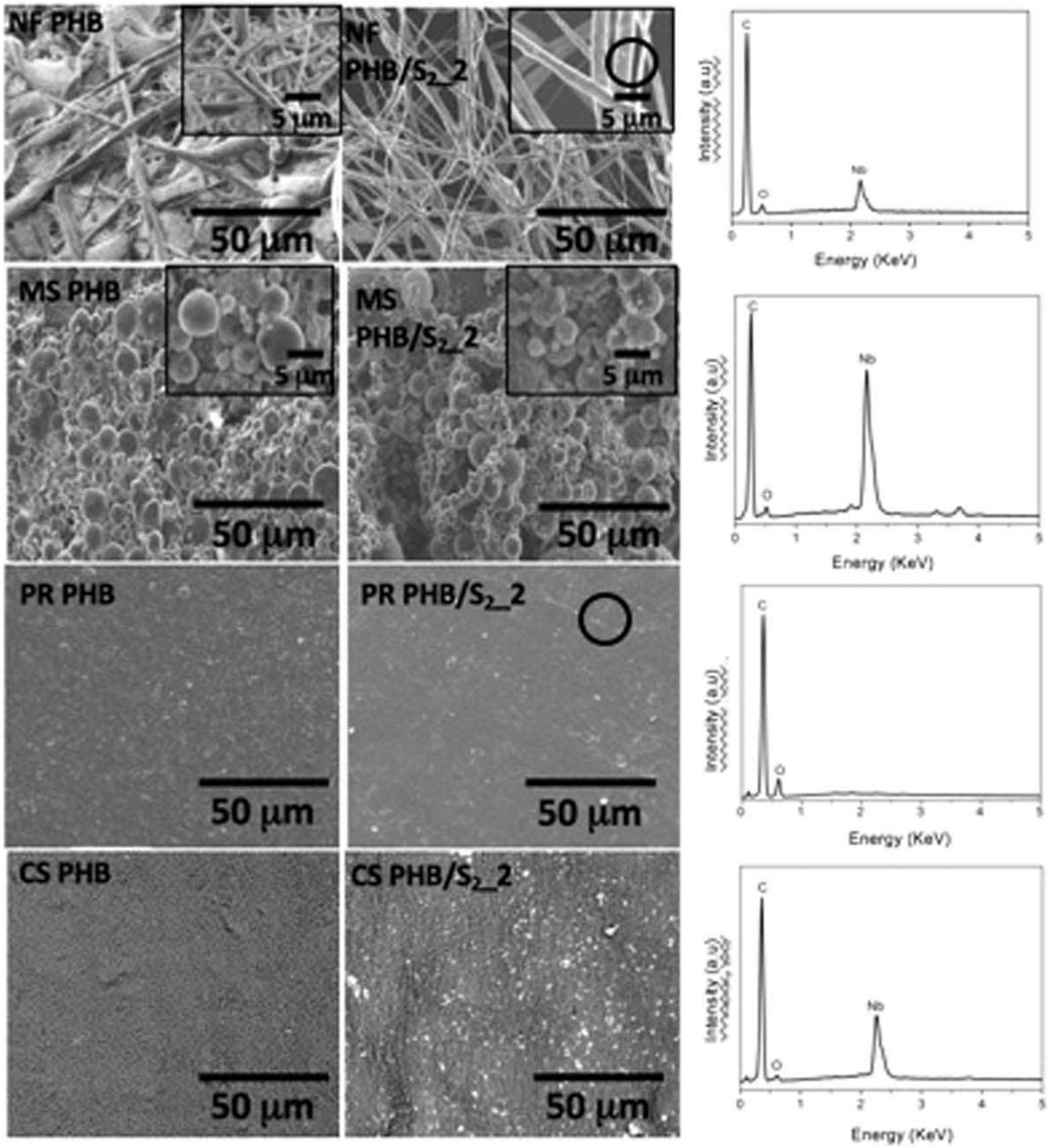

Figure 1. SEM images of the catalytic system PHB/S_2_2 in the form of nanofibers (NF), microspheres (MS), thermo-processed films (PR), and cast films (CS). The EDS spectra are related to the images that show nanoparticles incorporated in the polymer matrix. [Color figure can be viewed at wileyonlinelibrary.com]

EDS spectra verify the presence of the niobium compound in the nanocomposite PHB/S_2_2 MS, as indicated by an intense signal.

The images obtained from the surface were similar for the samples of PHB subjected to thermal processing, PHB, and PR PHB/S_2_2. However, it was necessary to conduct chemical mapping of the sample fracture to permit identification of nanocompounds of niobium, which were not revealed by EDS spectra. The images are shown in Figure 2.

The sizes of the niobium oxyhydroxide nanoparticles are of the order of 200 nm, and the nanoparticles are well dispersed and distributed in the polymer matrix, as observed in the chemical mapping SEM images by backscattered electrons. Mixing of the nanoparticles with the PHB matrix using a rheometer is more efficient than other methods. The melt processing may have caused the reduction in the size of the agglomerated inorganic particles due to the effect of shear stress exerted during the processing. Thus, it was not possible to identify the nanoparticles in the SEM images by secondary electrons.

The SEM images of PHB CS and PHB/S_2_2 CS surfaces are shown at the bottom of Figure 1. The presence of niobium agglomerates was observed on the surface of the polymer matrix

10974628, 2018, 7, Downloaded from https://onlinelibrary.wiley.com/doi/10.1002/app.45836 by INPI - Instituto Nacional da Propriedade Industrial, Wiley Online Library on [18/06/2023]. See the Terms and Conditions (https://onlinelibrary.wiley.com/terms-and-conditions) on Wiley Online Library for rules of use; OA articles are governed by the applicable Creative Commons License

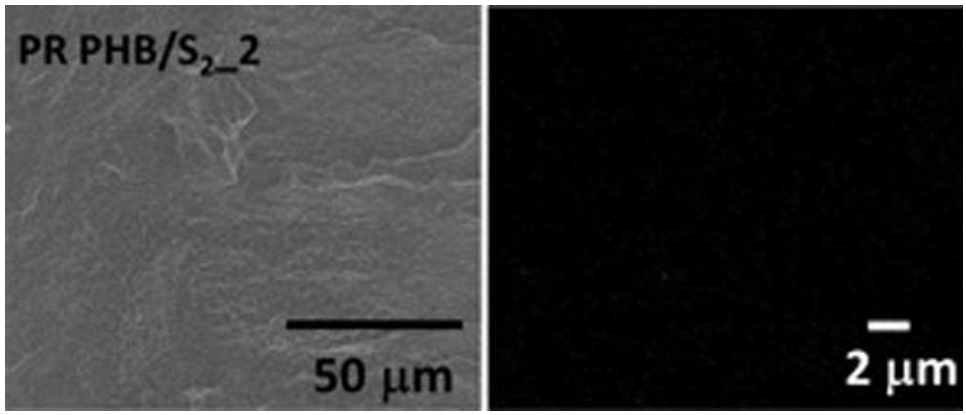

Figure 2. SEM images using backscattered electrons to generate the chemical map of the sample PR PHB/S_2_2. [Color figure can be viewed at wileyonlinelibrary.com]

in PHB/S_2_2 CS films, as confirmed by the EDS spectrum. The light points in the PHB/S_2_2 CS image were not observed in the PHB CS image. As described in a previous work,[33] niobium nanoparticles are distributed in the surface and bulk of PHB. However, the bulk of the particles is smaller than the surface. In the surface, the nanoparticle cluster size has a wide range, although most particles have a size of approximately $\leq$1 μm.

The chemical interactions between the polymer matrix and niobium nanoparticles were investigated using FTIR, and the spectra are shown in Figures 3(a,b). The spectra profiles of pure PHB and nanocomposites are typical of PHB. The main bands can be observed in the regions: (1) 1720 cm^{-1}, resulting from the stretching vibration of C═O of the ester group; (2) 1230 and 1279 cm^{-1} are associated from the stretching vibration of C—O—C.

The bands at approximately 1380 and 980 cm^{-1} are attributed to deformation of CH_3 and C—H groups, respectively, which are assigned to the ester group present in the crystalline polymer phase.[34] The FTIR spectra of the PHB/oxyhydroxide niobium nanocomposites demonstrate the predominance of bands associated with the polymeric matrix, due to the lower content of nanoparticles. To verify possible chemical interactions among the components of the materials, the bands in the carbonyl region of the PHB group (1720 cm^{-1}) were deconvoluted and mathematically adjusted using Gaussian functions, as shown in Figure 4.

After deconvolution and adjustment by Gaussian functions of the spectral region associated with the PHB carbonyl group, the presence of three bands is observed. The bands with maximum wavenumbers at 1716 and 1739 cm^{-1} are attributed to the stretching vibrations of the carbonyl groups of the crystalline and amorphous regions, respectively, and the band of low intensity at 1687 cm^{-1} is attributed to νC═O groups involved in interactions associated with the crystalline phase.[34,35] The addition of niobium oxyhydroxide in the polymer matrix did not cause significant shifts in the bands associated with the PHB carbonyl group [Figure 4(b)]. Nevertheless, the *R* ratio, that is, the area under the bonded carbonyl band divided by the total area of the carbonyl group, indicates the degree to which the carbonyl groups participate in hydrogen bonds. Thus, the higher the proportion of bonded carbonyls is, the higher is the *R* ratio. The *R* ratio was calculated for all samples of pure PHB and the nanocomposites prepared as NF, MS, PR, and CS, and the data are shown in Table I. The *R* ratios of all

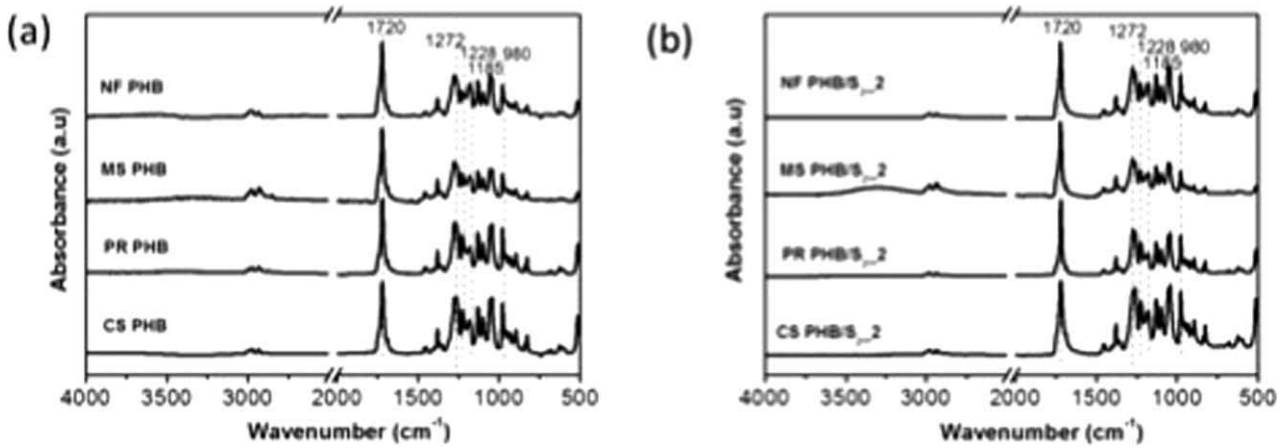

Figure 3. FTIR spectra of (a) PHB and (b) nanocomposites obtained by nanofibers (NF), microspheres (MS), thermos-processed films (PR), and cast films (CS).

1097462x, 2018, 7, Downloaded from https://onlinelibrary.wiley.com/doi/10.1002/app.45836 by INPI - Instituto Nacional da Propriedade Industrial, Wiley Online Library on [18/06/2023]. See the Terms and Conditions (https://onlinelibrary.wiley.com/terms-and-conditions) on Wiley Online Library for rules of use; OA articles are governed by the applicable Creative Commons License

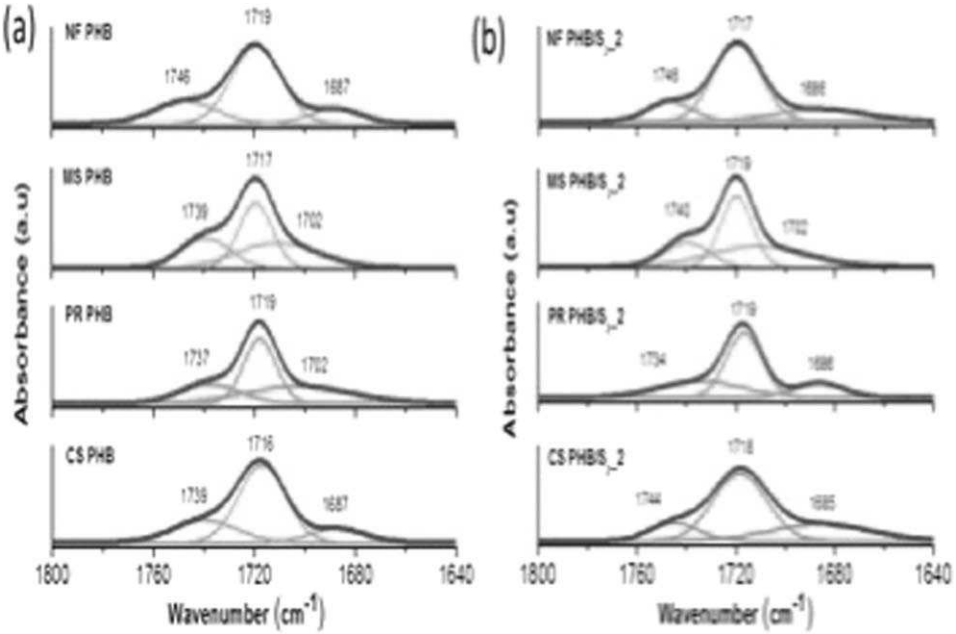

Figure 4. Band deconvolution curves associated with carbonyl FTIR–ATR spectra for different samples of PHB and PHB nanocomposite/S_2_2. [Color figure can be viewed at wileyonlinelibrary.com]

nanocomposites are higher than those of pure PHB prepared under similar conditions. This result may be related to the formation of hydrogen bonds between the OH groups of niobium oxyhydroxide and the carbonyl groups of PHB. This was also noted by Roa *et al.*,[35] who investigated the interaction of the PHB polymer and polyethylene glycol of low molecular weight, and Sadeghi *et al.*[36] have studied the incorporation of silica nanoparticles (0–30 wt %) into a polyurethane matrix.

The effect of the preparative method on the thermal stability of the pure PHB and nanocomposites was evaluated using thermogravimetric analysis. The curves obtained are shown in Figure 5, in addition to the derivatives of the TGA.

The analysis of the thermogravimetric curves verified that the weight loss of the materials occurs in one step. This can be attributed to random chain scission of PHB and hence its thermal degradation.[37] The loss of volatile compounds at temperatures lower than 200 °C is not significant, indicating the absence of residual compounds. Solvents were used in the preparation of films through casting and electrospinning processes, but they were removed efficiently.

In general, the method of preparation of the materials and the addition of inorganic nanoparticles are responsible for the modification of the thermal degradation of PHB. The derivatives of the TG, that is, DTG (Figure 5) curves were used to identify the initial temperature (T_{onset}) and the maximum degradation rate (T_{MS}) of the weight loss phases of materials, as shown by the data in Table II.

Comparing the pure PHB samples prepared by different methods, it was observed that the material obtained by the electrospinning method has lower thermal stability, with a weight loss in the range 204–281 °C and T_{MS} at 260 °C. The films obtained by thermo-processing, casting, and MS showed weight loss ranges between 226 and 300 °C, 232 and 300 °C, and 223 and 288 °C, respectively. The electrospinning method promotes the formation of fibers by the application of an electric field using a high voltage, leading to a polymeric structure different from the others.

The materials obtained by electrospinning, casting and MS showed increased thermal stability after the addition of niobium nanoparticles because T_{onset} was shifted to higher temperatures, as seen in Table II. A similar behavior is observed when comparing the T_{MS} of these samples. PR PHB/S_2_2 showed a slight increase in thermal stability, in which T_{onset} ranged from 226 to 232 °C, and there was no significant change in T_{MS}. These

Table I. Parameters Calculated from the Curves Obtained by Deconvolution of the Bands in the C═O Regions Related to Polyhydroxybutyrate (PHB) and PHB Nanocomposite/S_2_2

Samples	*R*	Samples	*R*
CS PHB	0.84 (±0.01)	PR PHB	0.74 (±0.03)
CS PHB/S_2_2	0.90 (±0.03)	PR PHB/S_2_2	0.83 (±0.01)
NF PHB	0.78 (±0.03)	MS PHB	0.75 (±0.03)
NF PHB/S_2_2	0.84 (±0.02)	MS PHB/S_2_2	0.81 (±0.01)

10974628, 2018, 7, Downloaded from https://onlinelibrary.wiley.com/doi/10.1002/app.45836 by INPI - Instituto Nacional da Propriedade Industrial, Wiley Online Library on [18/06/2023]. See the Terms and Conditions (https://onlinelibrary.wiley.com/terms-and-conditions) on Wiley Online Library for rules of use; OA articles are governed by the applicable Creative Commons License

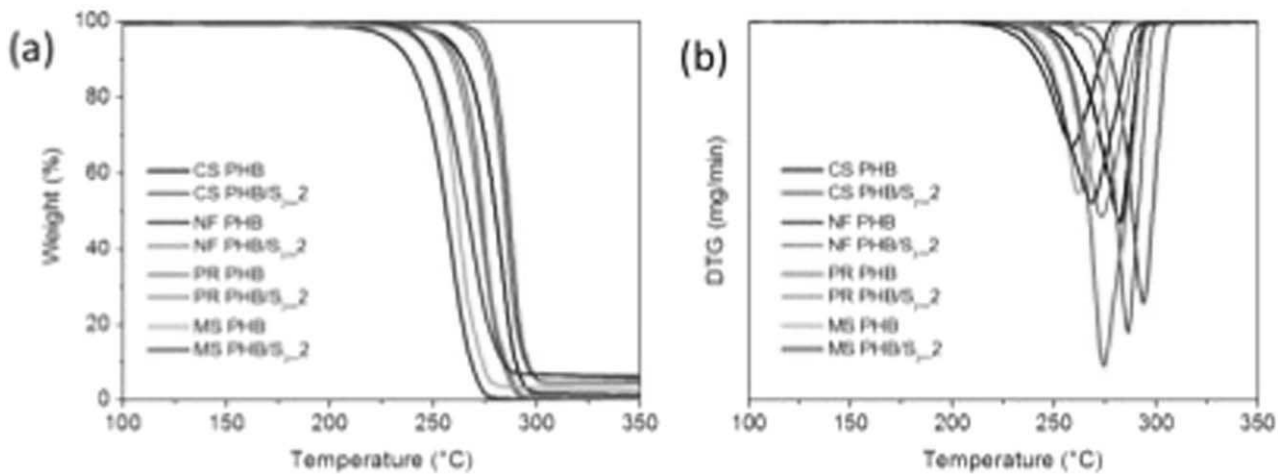

Figure 5. TGA curves and DTG of pure PHB and nanocomposites PHB/S_2_2, obtained by different methods of preparation. [Color figure can be viewed at wileyonlinelibrary.com]

results demonstrate that the incorporation of niobium oxyhydroxide increases the thermal stability of the PHB. Because the niobium oxyhydroxide is more thermally stable than the matrix, it acts as a thermal barrier to prevent heat transfer through the polymer matrix. This type of effect has been reported previously for other biodegradable polymers.[38] Similar observations were reported in the study of thermal stability of the composites of PHB and ZnO[37] and PHB and carbon nanotubes,[28] in which the nanoparticles act as a barrier to polymer degradation. It is important to note that the increase of T_{onset} and T_{MS} due to the addition of niobium nanoparticles is higher than that of the composites PHB and Ag_2S,[39] PHB and Fe_3O_4,[40] PHB and inorganic nanotubes of WS2[41] and hybrid materials of PHB and montmorillonite.[8]

The properties of semicrystalline polymers such as PHB can be determined by the crystallization mechanisms, which vary depending on the preparative method.[42] PHB is highly crystalline because its slow crystallization kinetics result in the formation of large crystals, leading to a brittle material. Therefore, the study of the melting profile is essential to understand the properties of the material and its relationship with the processing method. The DSC curves related to the second run of pure PHB and nanocomposites PHB/S2_2 are shown in Figure 6.

Table II. Parameters of Thermal Analysis of PHB and PHB/S_2_2 Composites

	Degradation		
Samples	T_{onset}	T_{MS}	T_{endset}
CS PHB	232	283	300
CS PHB/S_2_2	264	295	315
NF PHB	204	260	281
NF PHB/S_2_2	250	287	305
PR PHB	226	275	300
PR PHB/S_2_2	232	273	303
MS PHB	223	262	288
MS PHB/S_2_2	221	268	295

Regarding the heating obtained after crystallization, shown in Figure 6, it is observed that pure PHB and nanocomposites PHB/S_2_2 have a double melting peak (T_{m_1} and T_{m_2}) independent of the preparative method used. Multiple peaks are attributed mainly to (1) melting, recrystallization and re-melting during the DSC scan; (2) crystals of different families, sizes, lamellar thicknesses, and imperfections; (3) the presence of more than one type of crystal, that is, polymorphism; or (4) structural changes in the conformations of chains.[43,44] The profile of the melt peaks showed in the DSC curve is similar to either pure polymers and nanocomposites regardless of preparation methods chosen, PR or NF; differently when compared the MS and CS samples showing changes.

The peak appearing at lower temperature (T_{m_1}) goes to a higher temperature than those of the materials CS PHB/S_2_2 and MS PHB/S_2_2. The main effects responsible for this type of displacement are imperfections, smaller sized crystals, and/or decreased thickness. The fusion process, recrystallization, and re-melting contribute to a lesser extent because the double peak is observed in the first scan (not shown here). However, the occurrence of an exothermic event, recorded at 70 °C only in the curves of the materials obtained via casting, is indicative of crystallization during the heating. The chains that were not fully crystallized in the cooling acquire mobility and are organized from the existing crystals. Table III shows the thermal properties obtained by DSC curves, including the melting temperature (T_{m_1} and T_{m_2}), melting enthalpy (ΔH_m) and degree of crystallinity (X_c) of all samples.

PHB materials obtained by thermo-processing (PR PHB) and casting (CS PHB) showed the melting temperatures T_{m_1} and T_{m_2} of approximately 158 and 169 °C, respectively. There are no significant differences in the melting temperatures for CS PHB/S_2_2, PR PHB/S_2_2, and MS PHB/S_2_2 compared to pure PHB. However, in the film obtained by electrospinning (NF PHB), the peaks are shifted to lower values than other pure PHB

1097-4628, 2018, 7, Downloaded from https://onlinelibrary.wiley.com/doi/10.1002/app.45836 by INPI - Instituto Nacional da Propriedade Industrial, Wiley Online Library on [18/06/2023]. See the Terms and Conditions (https://onlinelibrary.wiley.com/terms-and-conditions) on Wiley Online Library for rules of use; OA articles are governed by the applicable Creative Commons License

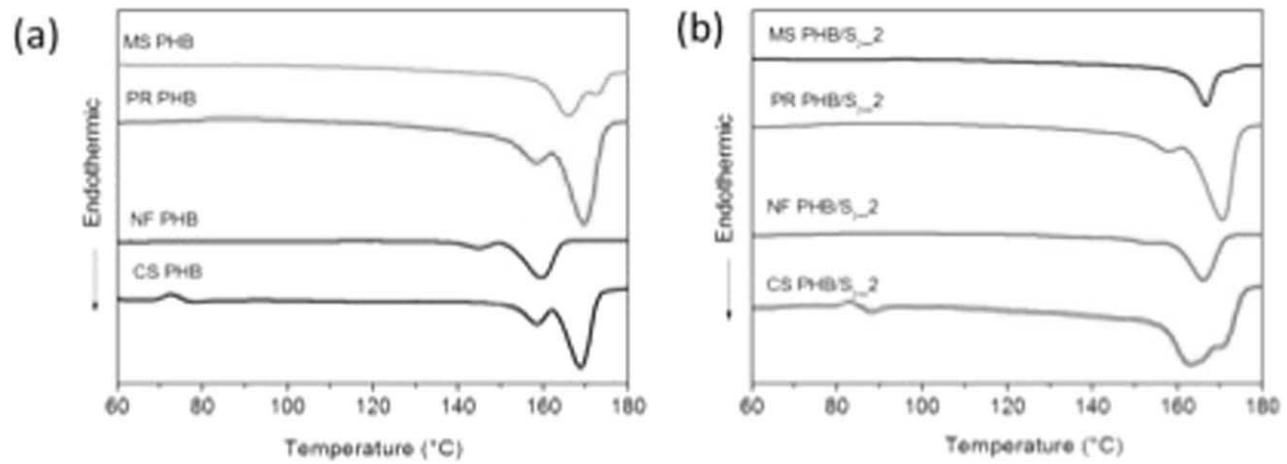

Figure 6. DSC curve for the second run of PHB (a), nanocomposites of PHB/S2_2 (b) prepared by electrospinning, microspheres, thermo-processing, and casting. [Color figure can be viewed at wileyonlinelibrary.com]

samples (PR PHB and CS PHB) and are found at $T_{m_1} \sim 145\,^{\circ}C$ and $T_{m_2} \sim 159\,^{\circ}C$. The semicrystalline materials subjected to cold stretching, as in the electrospinning process (NF PHB), have their helical macromolecular structure (α form) converted to a zig-zag-conformation planar (β form) phase with more disordered characteristics, as observed by Kim *et al.*[44] The authors reported the fusion of the β form at 165 °C, lower than the α form temperature, similar to the results obtained in this work. When comparing the samples NF_PHB and NF_PHB/S_2_2 the addition of S_2 in the PHB NF led to an increase in both temperatures, T_{m_1} and T_{m_2}, to 153 and 166 °C, respectively.

This result indicates that the presence of inorganic nanoparticles least favors the formation of imperfect crystals. The analysis of the curves shows that the β conformation is preferred in both the pure polymer and nanocomposite materials obtained via electrospinning. The width of the NF is smaller than the average size of the PHB crystals obtained by crystallization through CS PHB (casting) or PR PHB (thermo-processing). Thus, in the process of electrospinning, smaller crystals are forced to be formed, and the β phase is favored due to the stretching of chains.

The degree of crystallinity of the materials is also affected by the preparative methods of PHB and the addition of niobium oxyhydroxide, as shown in Table III. Samples of PHB, NF PHB, MS PHB, and PR PHB show similar degrees of crystallinity of ~50 and 60%, respectively, although the α form is predominant in the first two compounds, contrary to the material obtained by electrospinning. CS PHB showed a higher crystallinity close to 87% and also exhibited the preferred α form.

The fast cooling of samples obtained from the melt causes the formation of heterogeneous crystals, leading to decreased crystallinity. The chains have less mobility, and the crystallization process occurs rapidly. Furthermore, the strands may suffer breakage due to shear and elevated temperature during processing, resulting in smaller chains that contribute to imperfections in crystals. Because the materials are obtained through casting, evaporation of the solvent at room temperature allows slow crystallization of the polymer chains, favoring high crystallinity.

The presence of niobium oxyhydroxide in the PHB matrices subjected to different processing modes causes the loss of crystallinity in the materials, as indicated in Table III. Thus, the particles of niobium oxyhydroxide restrict the movement of the polymer chain during the growth stage of crystals and can also act as nucleating agents, causing uncontrolled growth of crystals in the matrix–particle interface. As a result, the PHB crystals begin to grow on the surface of the particle and the crystal size is reduced due to the increased number of nuclei formed.[45] This result was also observed by Liao *et al.*,[46] who studied the incorporation of carbon nanotubes with multiple layers in the PHB matrix, and Puglia *et al.*,[8] who studied the effect of clay incorporation in modifying the PHB crystallization kinetics.

Table III. Thermal Properties Obtained from the DSC Curves for the Pure PHB and Nanocomposite and PHB/S2_2 Sample Prepared by Electrospinning (NF), Microsphere (MS), Thermo-Processing (PR), and Casting (CS)

Samples	T_{m_1} (°C)	T_{m_2} (°C)	ΔH_m (J/g)	X_{cDSC} (%)	Samples	T_{m_1} (°C)	T_{m_2} (°C)	ΔH_m (J/g)	X_{cDSC} (%)
NF PHB	145	159	84.02	57	NF PHB/S_2_2	153	166	80.47	55
MS PHB	165	172	76.15	52	MS PHB/S_2_2	166	173	61.80	42
PR PHB	158	169	92.46	63	PR PHB/S_2_2	158	171	74.59	51
CS PHB	158	169	117.02	80	CS PHB/S_2_2	163	171	103.10	72

10974628, 2018, 7, Downloaded from https://onlinelibrary.wiley.com/doi/10.1002/app.45836 by INPI - Instituto Nacional da Propriedade Industrial, Wiley Online Library on [18/06/2023]. See the Terms and Conditions (https://onlinelibrary.wiley.com/terms-and-conditions) on Wiley Online Library for rules of use; OA articles are governed by the applicable Creative Commons License

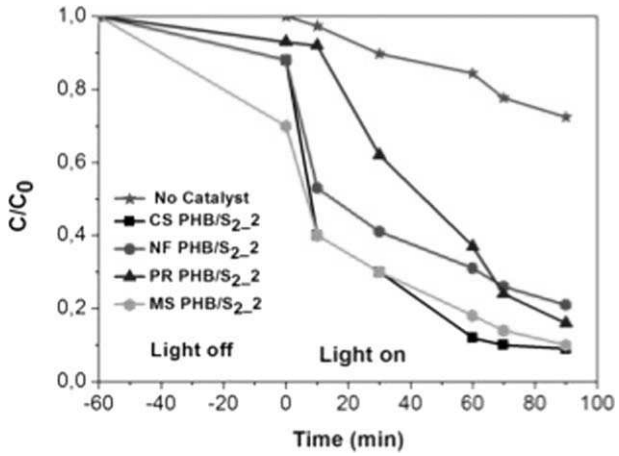

Figure 7. Kinetic curves for removal of aqueous methylene blue dye by PHB/S_2_2 composites prepared by casting (CS), microsphere (MS), thermal processing (PR), and eletrospinning (NF) methods. [Color figure can be viewed at wileyonlinelibrary.com]

The ability of niobium oxyhydroxide to catalyze the process of removal of methylene blue from aqueous media has been demonstrated in previous works.[29,47,48] Niobium-based PHB/oxyhydroxide nanocomposites (S_2) prepared by different methods have been employed in the photocatalytic process to remove methylene blue dye from solution. Importantly, the immobilization of the catalyst in the polymer allows the easy removal of the aqueous medium, presenting the possibility of reusability in the process of photocatalysis.[22,33] The removal of methylene blue dye was monitored using UV–vis spectroscopy at 664 nm. Kinetic curves obtained for the removal of the dye solution using the PHB/S2_2 composites with different morphologies are shown in Figure 7.

The range −60–0 min represents the time of dye adsorption by the PHB-based nanocomposites. In this range, the UV light remained off. Then, at 0 min, the UV light was turned on to start the photocatalytic reaction. The removal of dye by adsorption is the highest on MS_PHB, reaching ∼30%, and lowest on PR_PHB, with a value of <5%. As demonstrated in a previous work, the dye adsorption increases with higher S2 content, reaching a limit.[22] However, in this case, the S_2 content was the same in all the nanocomposites. The adsorption is probably related to the ability of the matrix to cover the niobium nanoparticles. As shown in Table I, the *R* parameter changes from 0.73 to 0.84 when comparing the samples PHB_PR and PHB/S_2_PR, respectively. This variation is higher than any other samples prepared through other methods and indicates more nanoparticle–polymer matrix interactions.

Figure 8. Photography of the CS PHB/S2_2 film removed from aqueous medium. [Color figure can be viewed at wileyonlinelibrary.com]

The EDS spectra corroborate these data because the niobium signal is not observed. Niobium nanoparticles that are better dispersed in the matrix by coating in the polymer exhibit lower adsorption. Additionally, the niobium nanoparticle content in the surface contributes to increased MS absorption. This point can be related to the highest intensity observed in the EDS spectrum compared with the others, rather than the smaller influence of nanoparticles on thermal properties.

The photocatalytic reactions were initiated as soon as the light was turned on. Although the photolysis process occurred ("no catalyst" curve), the significant change in the kinetic curves of dye removal in the presence of all tested samples demonstrates the photocatalytic contribution. As seen in Figure 7, the film obtained via casting (CS) stood out, with quick removal of the dye color. After 10 min of reaction, there is a removal of ∼60%, which becomes constant after 70 min of reaction. Removal of the methylene blue using CS PHB/S_2_2 was close to 90%. The results of DSC, ΔX_{cDSC} (X_{cDSC}PHB − X_{cDSC}PHB/S_2_2) and the curve profile indicate that the largest change in the structure of the crystalline region of PHB CS is decreased uniformity. One hypothesis is that the amorphous areas become more scattered, allowing higher mobility of the polymer chains and leading to greater exposure of the catalyst particles throughout the process.

Despite the removal of 60% of dye in 10 min by MS PHB/S_2_2, this sample presents worse performance in the photocatalytic processes after discounting dye absorption. Similar results can be observed for NF PHB/S_2_2. Finally, after 10 min, the rate of discoloration of the solution with PR PHB/S_2_2 increases compared with the others. This effect can be justified by the smaller particle size, as shown by the SEM images in Figure 2. The favoring of photocatalysis by reducing the catalyst size is a known effect.[49,50] Though PR PHB/S_2_2 nanocomposite has a slightly lower performance than CS PHB/S_2_2 up to 90 min, it has the advantage of being produced on an industrial scale.

It is noteworthy that the nanocomposites containing PHB/niobium nanoparticles are active in the photocatalysis reaction and are easily removed from the aqueous medium (Figure 8).

CONCLUSIONS

In this work, nanocomposites based on PHB and niobium oxyhydroxide (S2) with different morphologies were developed. SEM analysis suggests that the distribution and dispersion of nanoparticles in the PHB matrix are dependent on the preparative method. The chemical interaction between the components may be due to that between PHB and the OH groups of niobium nanoparticles. DSC and TG show that the incorporation of inorganic nanoparticles of niobium in PHB increases the thermal stability of the polymer, and these nanoparticles act as nucleating agents, directly affecting the crystallinity of PHB by heterogeneous nucleation.

The formed nanocomposites are effective in the removal of the methylene blue dye in an aqueous medium in the presence of

10974628, 2018, 7, Downloaded from https://onlinelibrary.wiley.com/doi/10.1002/app.45836 by INPI - Instituto Nacional da Propriedade Industrial, Wiley Online Library on [18/06/2023]. See the Terms and Conditions (https://onlinelibrary.wiley.com/terms-and-conditions) on Wiley Online Library for rules of use; OA articles are governed by the applicable Creative Commons License

UV radiation via photocatalysis. This behavior is attributed to the presence of niobium nanoparticles immobilized in the polymer, which present peroxo groups on their surface, thus increasing photocatalytic activity. The adsorption process is dependent mostly on the nanoparticle content on the surface of the materials, while the photocatalysis depends on the nanoparticles size.

ACKNOWLEDGMENTS

This work is a collaboration research project of members of the Rede Mineira de Química (RQ-MG) supported by FAPEMIG (Project: CEX-RED-00010-14). This work was supported by grants from CNPq, FAPEMIG, and CAPES.

REFERENCES

1. Fabra, M. J.; Lopez-Rubio, A.; Lagaron, J. M. *J. Food Eng.* **2014**, *127*, 1.
2. Vogelsanger, N.; Formolo, M. C.; Pezzin, A. P. T.; Schneider, A. L. D. S.; Furlan, S. A.; Bernardo, H. P.; Pezzin, S. H.; Pires, A. T. N.; Duek, E. A. D. R. *Mater. Res.* **2003**, *6*, 359.
3. Arrieta, M. P.; Samper, M. D.; López, J.; Jiménez, A. *J. Polym. Environ.* **2014**, 460.
4. El-Toony, M. M.; Abdel-Hady, E. E.; El-Kelsh, N. A. *Electrochim. Acta* **2014**, *150*, 290.
5. Yang, K.-K.; Wang, X.; Wang, Y.-Z. *Rev. Lit. Arts Am.* **2007**, *13*, 485.
6. Angelini, S.; Cerruti, P.; Immirzi, B.; Santagata, G.; Scarinzi, G.; Malinconico, M. *Int. J. Biol. Macromol.* **2014**, *71*, 163.
7. Wei, L.; Liang, S.; McDonald, A. G. *Ind. Crops Prod.* **2015**, *69*, 91.
8. Puglia, D.; Fortunati, E.; D'Amico, D. a.; Manfredi, L. B.; Cyras, V. P.; Kenny, J. M. *Polym. Degrad. Stab.* **2014**, *99*, 127.
9. Avella, M.; Martuscelli, E.; Raimo, M. *J. Mater. Sci.* **2000**, *35*, 523.
10. Sperling, L. H. Introduction to Physical Polymer Science, 4a ed.; John Wiley & Sons, Inc: Hoboken, NJ, **2006**; Vol. *78*.
11. Yang, D.; Zhang, J.; Xue, J.; Nie, J.; Zhang, Z. *J. Appl. Polym. Sci.* **2013**, *127*, 2867.
12. Mottin, A. C.; Ayres, E.; Oréfice, R. L.; Câmara, J. J. D. *Mater. Res.* **2016**, *19*, 57.
13. Tanaka, F.; DOI, Y.; Iwata, T. *Polym. Degrad. Stab.* **2004**, *85*, 893.
14. da Silva Pinto, C. E.; Arizaga, G. G. C.; Wypych, F.; Ramos, L. P.; Satyanarayana, K. G. *Compos. Part A: Appl. Sci. Manuf.* **2009**, *40*, 573.
15. Containing, M.; Bazzo, G. C.; Lemos-senna, E.; Gonçalves, M. C.; Pires, A. T. N. *J. Braz. Chem. Soc.* **2008**, *19*, 914.
16. Francis, L.; Meng, D.; Knowles, J.; Keshavarz, T.; Boccaccini, A. R.; Roy, I. *Int. J. Mol. Sci.* **2011**, *12*, 4294.
17. Siemann, U. *Prog. Colloid Polym. Sci.* **2005**, *130*, 1.
18. Anbukarasu, P.; Sauvageau, D.; Elias, A. *Sci. Rep.* **2015**, *5*, 17884.
19. Torres, J. D.; Faria, E. A.; SouzaDe, J. R.; Prado, A. G S. *J. Photochem. Photobiol. A Chem.* **2006**, *182*, 202.
20. Ramier, J.; Bouderlique, T.; Stoilova, O.; Manolova, N.; Rashkov, I.; Langlois, V.; Renard, E.; Albanese, P.; Grande, D. *Mater. Sci. Eng. C* **2014**, *38*, 161.
21. Bonartsev, A. P.; Livshits, V. A.; Makhina, T. A.; Myshkina, V. L.; Bonartseva, G. A.; Iordanskii, A. L. *eXPRESS Polym. Lett.* **2007**, *1*, 797.
22. Yew, S. P.; Tang, H. Y.; Sudesh, K. *Polym. Degrad. Stab.* **2006**, *91*, 1800.
23. Sridewi, N.; Tan, L. T.; Sudesh, K. *Clean* **2011**, *39*, 265.
24. Sudesh, K.; Sridewi, N.; Lee, Y. F. *Int. J. Photoenergy* **2011**, *2011*, 1.
25. Esteves, A.; Oliveira, L. C. A.; Ramalho, T. C.; Goncalves, M.; Anastacio, A. S.; Carvalho, H. W. P. *Catal. Commun.* **2008**, *10*, 330.
26. Oliveira, H. S.; Almeida, L. D.; Freitas, V. A. A. D.; Moura, F. C. C.; Souza, P. P.; Oliveira, L. C. A. *Catal. Today* **2015**, *240*, 176.
27. Nogueira, A. E.; Ramalho, T. C.; Oliveira, L. C. A. *Top. Catal.* **2011**, *54*, 270.
28. Parra, D. F.; Fusaro, J.; Gaboardi, F.; Rosa, D. S. *Polym. Degrad. Stab.* **2006**, *91*, 1954.
29. Ferraz, W.; Oliveira, L. C. A.; Dallago, R.; Conceição, L. d. *Catal. Commun.* **2007**, *8*, 131.
30. Oliveira, L. C. A.; Portilho, M. F.; Silva, A. C.; Taroco, H. A.; Souza, P. P. *Appl. Catal. B Environ.* **2012**, *117–118*, 29.
31. Parra, D. F.; Rosa, D. S.; Rezende, J.; Ponce, P.; Lugão, A. B. *J. Polym. Environ.* **2011**, *19*, 918.
32. Sombatmankhong, K.; Suwantong, O.; Waleetorncheepsawat, S.; Supaphol, P. *J. Polym. Sci. Part B: Polym. Phys.* **2006**, *44*, 2923.
33. Heitmann, A. P.; Patrício, P. S. O.; Coura, I. R.; Pedroso, E. F.; Souza, P. P.; Mansur, H. S.; Mansur, A.; Oliveira, L. C. A. *Appl. Catal. B Environ.* **2016**, *189*, 141.
34. Xu, J.; Guo, B. H.; Yang, R.; Wu, Q.; Chen, G. Q.; Zhang, Z. M. *Polymer (Guildf)* **2002**, *43*, 6893.
35. Roa, J. P. B.; Patrício, P. S. D. O.; Oréfice, R. L.; Lago, R. M. *J. Appl. Polym. Sci.* **2013**, *128*, 3019.
36. Sadeghi, M.; Mehdi Talakesh, M.; Ghalei, B.; Shafiei, M. *J. Membr. Sci.* **2013**, *427*, 21.
37. Díez-Pascual, A. M.; Díez-Vicente, A. L. *Int. J. Mol. Sci.* **2014**, *15*, 10950.
38. Ten, E.; Turtle, J.; Bahr, D.; Jiang, L.; Wolcott, M. *Polymer (Guildf)* **2010**, *51*, 2652.
39. Yeo, S. Y.; Tan, W. L.; Abu Bakar, M.; Ismail, J. *Polym. Degrad. Stab.* **2010**, *95*, 1299.
40. Sangsanoh, P. S. P. *Chiang Mai J. Sci.* **2014**, *41*, 676.
41. Naffakh, M.; Marco, C.; Ellis, G.; Cohen, S. R.; Laikhtman, A.; Rapoport, L.; Zak, A. *Mater. Chem. Phys.* **2014**, *147*, 273.
42. Mohamed El-Hadi, A. *Polym. Bull.* **2014**, *71*, 1449.
43. Gunaratne, L. M. W. K.; Shanks, R. A.; Amarasinghe, G. *Thermochim. Acta* **2004**, *423*, 127.

10974628, 2018, 7, Downloaded from https://onlinelibrary.wiley.com/doi/10.1002/app.45836 by INPI - Instituto Nacional da Propriedade Industrial, Wiley Online Library on [18/06/2023]. See the Terms and Conditions (https://onlinelibrary.wiley.com/terms-and-conditions) on Wiley Online Library for rules of use; OA articles are governed by the applicable Creative Commons License

44. Park, K. H.; Liang, Y.; Kim, S. H.; Lee, H. S. *Macromolecules* **2006**, *39*, 1832.

45. Botana, A.; Mollo, M.; Eisenberg, P.; Torres Sanchez, R. M. *Appl. Clay Sci.* **2010**, *47*, 263.

46. Liao, H.-T.; Wu, C.-S. *Des. Monomers Polym.* **2013**, *16*, 99.

47. Cardoso, F. P.; Nogueira, A. E.; Patrício, P. S. O.; Oliveira, L. C. A. *J. Braz. Chem. Soc.* **2012**, *23*, 702.

48. Yoon, H.; Joshi, B. N.; Na, S.; Choi, J.; Yoon, S. S. *Ceram. Int.* **2014**, *40*, 7567.

49. Colmenares, J. C.; Luque, R.; Campelo, J. M.; Colmenares, F.; Karpinski, Z.; Romero, A. A. *Materials (Basel)* **2009**, *4*, 2228.

50. Chaturvedi, S.; Dave, P. N.; Shah, N. K. *J. Saudi Chem. Soc.* **2012**, *16*, 307.

10974628, 2018, 7, Downloaded from https://onlinelibrary.wiley.com/doi/10.1002/app.45836 by INPI - Instituto Nacional da Propriedade Industrial, Wiley Online Library on [18/06/2023]. See the Terms and Conditions (https://onlinelibrary.wiley.com/terms-and-conditions) on Wiley Online Library for rules of use; OA articles are governed by the applicable Creative Commons License

Applied Catalysis B: Environmental 189 (2016) 141–150

Contents lists available at ScienceDirect

Applied Catalysis B: Environmental

journal homepage: www.elsevier.com/locate/apcatb

Nanostructured niobium oxyhydroxide dispersed Poly (3-hydroxybutyrate) (PHB) films: Highly efficient photocatalysts for degradation methylene blue dye

Ana P. Heitmann[a], Patrícia S.O. Patrício[b], Italo R. Coura[b], Emerson F. Pedroso[b], Patterson P. Souza[b], Herman S. Mansur[a], Alexandra Mansur[a], Luiz C.A. Oliveira[a,*]

[a] Department of Chemistry, Federal University of Minas Gerais, Av. Antônio Carlos 6627, Campus Pampulha, 31270-901 BH-MG, Brazil
[b] Department of Chemistry, Federal Center of Technological Education of Minas Gerais, CEFET-MG, Av. Amazonas 5253, 30421-169 BH-MG, Brazil

ARTICLE INFO

Article history:
Received 15 October 2015
Received in revised form 19 January 2016
Accepted 12 February 2016
Available online 15 February 2016

Keywords:
Photocatalysis
PHB
Niobium oxyhydroxide

ABSTRACT

In this work, nanostructured niobium oxyhydroxide was dispersed over poly (3-hydroxybutyrate) (PHB), which is a biopolymer, for application as a photocatalyst using visible and UV light. PHB films with different amounts of niobium oxyhydroxide were characterized by diffuse UV–vis reflectance spectroscopy, FTIR-ATR and SEM. The characterizations showed particles of the niobium compound well-dispersed on the polymeric matrix, thus modifying the bandgap value, which improved the photocatalysis process. The material showed excellent catalytic activity (approximately 100% degradation) for the oxidation of methylene blue dye considering the reaction in a continuous flow bath. Moreover, the polymer films were easily removed from the solution after the reaction and reused several times while retaining their high activity. ESI–MS studies showed that the dye removal occurs by the formation of reaction intermediates due to the successive hydroxylation of the dye structure, confirming that the reaction took place improved by photocatalytic conditions.

© 2016 Elsevier B.V. All rights reserved.

1. Introduction

Wastewater containing organic pollutants represents one of the main causes of environmental pollution, thus presenting a threat to human health and the ecosystem [1]. After their discharge into the environment, these contaminants present resistance to conventional chemical methods and physical removal [2]. Photocatalytic degradation has attracted great interest as a process for removing organic and inorganic contaminants from wastewater [3–5]. However, the cost and technical barriers involved have hampered the application of photocatalysis because the recovery of the catalyst from the aqueous medium, when possible, is time-consuming and expensive.

Niobium oxides are promising materials for use in various reactions such as hydration, esterification, condensation and heterogeneous photocatalysis in advanced oxidation processes due to their special properties, such as their high BET surface area, high selectivity, and acidic sites [6,7]. Niobium catalysts have been found to be efficient in the oxidation of organic compounds in the aqueous medium and organic photodegradation of pollutants in the presence of ultraviolet radiation or sunlight [8]. Furthermore, the niobium oxides can be combined with other metals, such as platinum, ruthenium and rhodium, to improve their performance in many catalytic processes [9]. With respect to photocatalysis, two questions are considered to be crucial for the proper application of technology on an industrial scale: (i) the radiation-absorbing capacity of the photocatalyst in the visible region and (ii) its recovery for reuse. The recovery of a catalyst with nanometric dimensions from an aqueous medium is a complicated process, and many times the catalyst must be combined with other materials to promote solid/liquid separation. The importance of the immobilization of the catalysts in a matrix or on a support for application in photocatalysis has been growing in recent years, mainly due to their ease of removal from the aqueous medium for reuse [10].

Immobilization may allow the light absorption to be optimized because a polymeric matrix containing the immobilized catalyst can be positioned on the surface of the liquid containing the pollutant to be degraded. In recent years, various polymeric supports for catalysts have been studied because they exhibit high stability in the aqueous medium, have a low cost and are chemically inert [11].

* Corresponding author.
E-mail address: luizoliveira@qui.ufmg.br (L.C.A. Oliveira).

http://dx.doi.org/10.1016/j.apcatb.2016.02.031
0926-3373/© 2016 Elsevier B.V. All rights reserved.

Among the studied catalyst-polymer systems reported, the literature highlights that the thin films of polyethylene/TiO_2 (PE/TiO_2) and polypropylene/TiO_2 (PP/TiO_2) used for methylene blue dye degradation in the presence of UV radiation have higher stabilities compared to the commercially available material for the same purpose [12]. The polyethylene terephthalate (PET/TiO_2) system used for oxidation of As (III) to As (V) and removal of As (V) from the aqueous medium in the presence of ferric oxyhydroxide (II) and sunlight presents major advantages such as the use of low cost materials in the process and the removal of 94% of As (V) in natural water in only 60 min [13]. The composite of polyaniline (PANI/TiO_2) used for the degradation of methylene blue in the presence of visible radiation exhibited a high catalytic efficiency, yielding approximately 80% removal of the analyte in only 90 min [14]. Recently, Ghosh et al. [15] presented an interesting study employing a conductive polymer (poly(diphenylbutadiyne) (PDPB)) directly as a photocatalyst for dye degradation in aqueous medium.

However, sophisticated and expensive methods for impregnating the catalyst on the matrix, such as the sol-gel process, *in situ* chemical polymerization, and the spray coating technique, makes the development of these materials expensive. Moreover, all investigated polymers are synthetic with a difficult degradation process when released into the environment. Studies involving renewable polymers and materials have become necessary due particularly to their biodegradability and lower toxicity to the environment [16,17].

In a pioneering work reported by Yew et al. [10] the polymeric system poly (3-hydroxybutyrate) PHB/TiO_2 was studied for the degradation of organic contaminants and antibacterial activity via photocatalytic sterilization. In the study, the authors used a high amount of titanium dioxide in the polymer matrix, approximately 57 wt%. PHB is a biopolymer produced from renewable sources, *i.e.*, from fermentation by certain micro-organisms. In addition to being naturally biodegradable, PHB shows some properties similar to those of synthetic polymers, especially polypropylene [18–20]. Materials with this characteristic are attractive, as they are assimilated and decomposed by microorganisms making them easily converted into simple and mineralized compounds [21].

In this work, we report the development of a new catalytic system based on a PHB polymer film containing up to 5 wt% of highly dispersed niobium oxyhydroxide. The materials were produced via casting with slow evaporation of the solvent. The photocatalytic activity of this material under UV and visible light for the degradation of methylene blue dye was tested. The characteristics of this material permitted the reactions to be tested in a continuous flow system.

2. Experimental

2.1. Materials and chemicals

The oxyhydroxide niobium (S_2) was prepared in accordance with previous work of our group [8]. The catalyst was obtained using $NH_4[NbO(C_2O_4)(H_2O)](H_2O)n$, donated by CBMM—Companhia Brasileira de Metalurgia e Mineração (Araxá, state of Minas Gerais, Brazil), NaOH (Sigma-Aldrich) and H_2O_2 30% v/v (Synth). For the preparation of the nanocomposites were used PHB (ca. 600 kDa) from PHB Industrial S/A. (Serrana-SP-Brazil), chloroform (Synth) and dimethylformamide (Synth).

2.2. Preparation of PHB/S_2 nanocomposite film

The PHB and PHB/S_2 films, shown in Fig. 1, were obtained via the casting technique. For the preparation of the films, PHB powder was solubilized in chloroform and dimethylformamide (DMF) with the addition of oxyhydroxide niobium (S_2) at concentrations of 1, 2, 3 and 5 wt%. The solution was placed under constant agitation and heating to approximately 55 °C for 4 h until complete dissolution was achieved. The mixture was poured into a glass Petri dish and the solvent was left to evaporate at room temperature for 72 h. Then, the samples were dried at 60 °C for 24 h.

2.3. Characterization of the materials

The structural properties of PHB and PHB/S_2 composites were investigated by various characterization techniques. The diffuse reflectance spectra of the materials were obtained using a Shimadzu 3550 UV–vis spectrophotometer coupled with a diffuse reflectance detector listed in the region from 200 to 800 nm. The reflectance data were converted to a reissued function (Eq. (1)) called the Kubelka-Munk function and is defined as:

$F(R) = \frac{(1-R)^2}{2R} = \frac{k}{s}$ (1)where in R is the absolute reflectance, and k is the coefficient of the absorption and s is the coefficient of scattering. The indirect bandgap calculation (Eq. (2)) was determined by the Tauc formalism, which was considered for only direct transitions with n = ½ [22].

$$\alpha h\nu^n = (F(R)) \times h\nu^n (2)$$

α is the absorption coefficient, h is Planck's constant, and ν is the frequency of the radiation.

The morphologies of the materials were characterized by scanning electron microscopy (SEM) using a JEOL scanning 840A model microscope operated at 7 kV. Chemical mapping was conducted using a Shimadzu model SSX-550 instrument operated at 15 kV. Infrared spectroscopy (FTIR) was realized in a Thermo Scientific spectrophotometer equipped with an attenuated total reflection accessory (micro-crystal ZnSe ATR with 300 mM) using a Cassegrain microscope (Centaurus, 10× magnification) in the reflection mode.

2.4. Catalytic tests

The catalytic tests were performed at 25 °C using 15 mL of methylene blue solution (20 mg L^{-1}) containing 0.5 g of polymer films with a stirring rate of 330 rpm using a mechanical stirrer for 10–120 min. A UV lamp (mercury vapor, λ = 254 nm- TOVALIGHT GLT) and visible radiation (dichroic lamp, λ > 400 nm- TOSCHIBRA) were used. The oxidation efficiency was monitored with a UV–vis

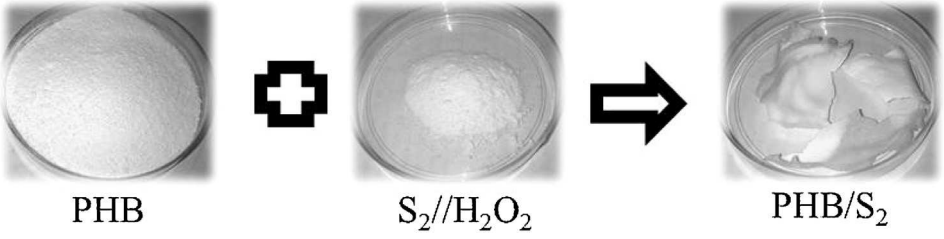

Fig. 1. Image of the PHB/S2 film obtained by casting.

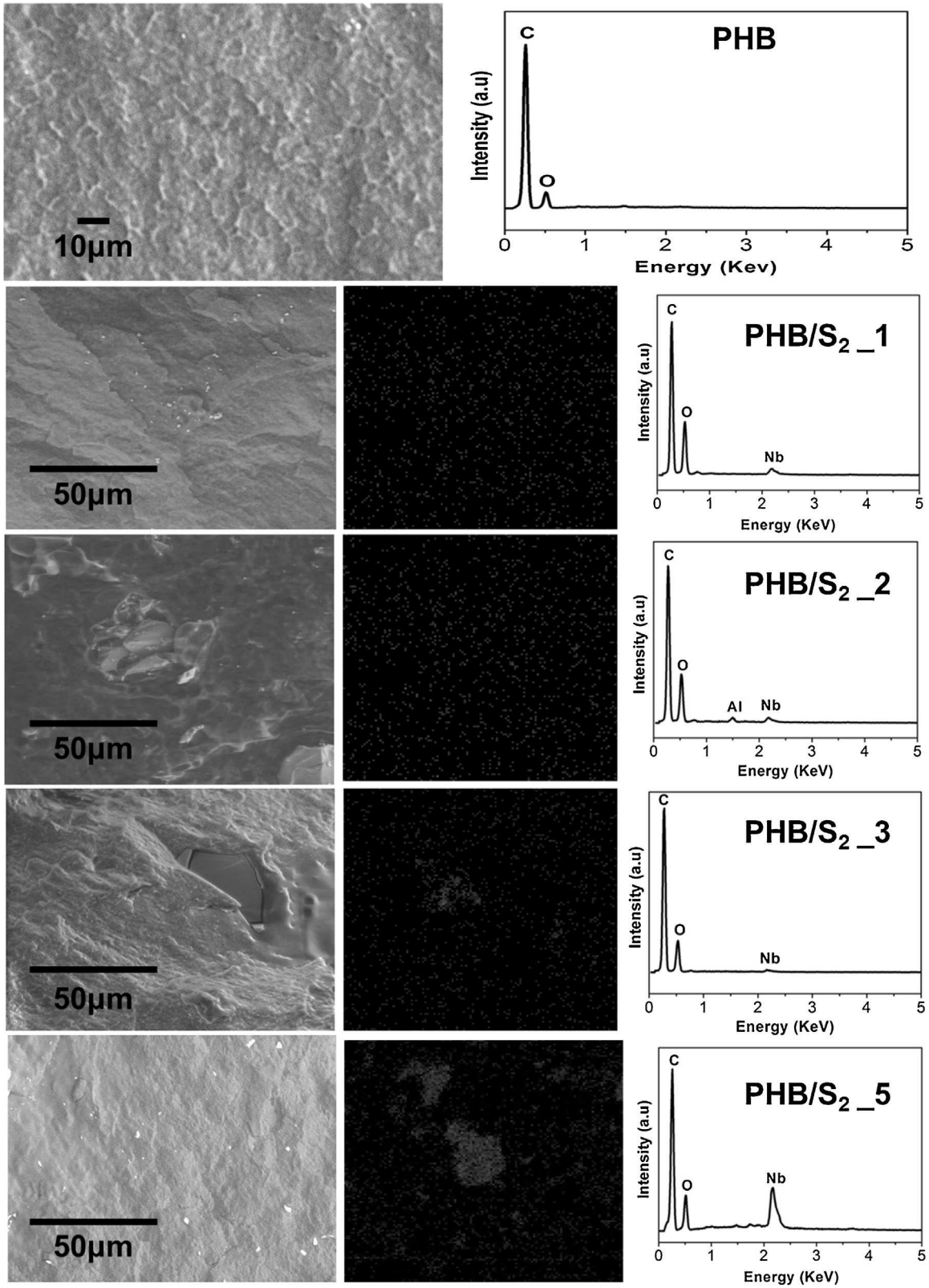

Fig. 2. SEM images: surface of the cryogenic fracture (secondary electron) of the PHB and nanocomposites PHB/S2_1, PHB/S2_2, PHB/S2_3 and PHB/S2_5 (left) and chemical mapping (electron backscattering) of nanocomposites films (middle). The EDS spectra of films (right) obtained focusing on the light regions in the SEM images by secondary electron.

spectrophotometer (Shimadzu, UV-1601 PC) at 664 nm, which is a characteristic wavelength of the methylene blue dye. To identify the intermediate chemical species formed during the oxidation of methylene blue, ESI–MS was used. For the tests in continuous flow, 5 g of polymeric films and 250 mL of methylene blue dye solution (20 mg L^{-1}) were employed. A PVC pipe was used as the photore-

Table 1
Band gaps of nanocompounds PHB/S_2 materials.

Materials	Bandgap value/eV
PHB/S2 _1	2.53
PHB/S2 _2	2.67
PHB/S2 _3	2.91
PHB/S2 _5	2.97
S2	3.00

actor. The PVC pipe was coated with various polymeric films that are flexible for introducing and were easily adhered to the surface of the photocatalyst. We used a peristaltic pump for circulating the dye solution at a flow of 60 L h^{-1}. The system used is shown in supporting information (Fig. S1).

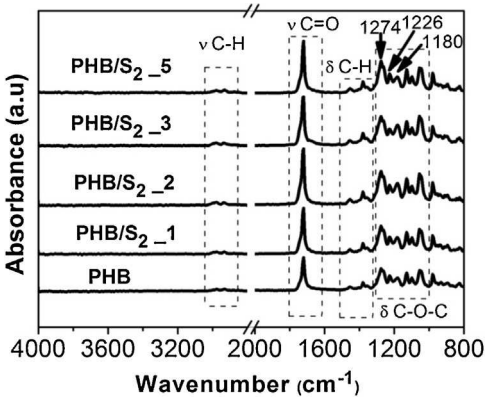

Fig. 3. FTIR-ATR spectra of the PHB film and 1–5 wt% composite PHB/S_2.

3. Results and discussion

3.1. Characterization of the materials

The materials were characterized by diffuse reflectance spectroscopy. The data obtained were converted to the Kubelka-Munk reference function (Eq. (1)) and are represented in Table 1.

S_2 has a bandgap value of 3.0 eV. To the composites containing 1, 2, 3 and 5 wt% niobium oxyhydroxide bandgap values increased with increasing niobium contents. According to Li et al. [23] incorporation into a support material will result in variation of the bandgap. Nevertheless, the bandgaps of PHB/S2 films show lower values than those with niobium oxyhydroxide particles. The composites can be excited to produce electron-hole pairs in the presence of visible and UV light, which can result in a high catalytic activity as reported by Li et al. [23]. The SEM/EDS technique was used to evaluate the morphologies and chemical compositions of the cryogenic fractures of PHB/S2 films (Fig. 2).

The SEM images shown in Fig. 2 correspond to the cryogenic fractures of pure PHB and PHB/S2 composites. The fracture profile is typical of brittle materials and characteristic of PHB. The SEM images show no significant differences in the film fracture patterns because they present similar formations of cracks. In the EDS spectra, focusing on the light regions observed in the sample fracture SEM images, 1–5% PHB/S2 showed a large amount of niobium, as opposed to that observed in the spectra for the dark region of the PHB matrix, similar to the pure PHB spectra (Fig. 2 right). In the EDS spectra of the PHB/S_2_2 was observed the presence of aluminum which may be attributed to some contamination in the preparation of nanocomposites.

It is suggested that the light phases in the SEM images are agglomerates of nanoparticles present in the polymer matrix. The images obtained by SEM and chemical mapping results indicate that good distributions of the agglomerates on the entire polymer matrix for all of the concentrations of niobium oxyhydroxide were obtained [24].

S2 was characterized by FTIR. The profile bands in spectra are typical of niobium oxyhydroxide with vibration about 3100 cm-1 related to bulk hydroxyl group present in this material [25]. This type of vibration is characteristic of an oxyhydroxide phase as described in our previous work [26,27]. Pure PHB and PHB/S_2 composites were investigated using FTIR-ATR (Fig. 3). The FTIR-ATR spectrum of the pure PHB is characterized by the presence of bands between 3000 and 2900 cm^{-1} related to the symmetrical stretching of the CH_3 group as well as bands from 1460 to 1380 cm^{-1} associated with asymmetric stretching and CH_2 groups. The bands that appear in the FTIR-ATR spectrum of PHB can be related to two primary components corresponding to the crystalline and amorphous phases.

The bands in the region of 1300–1100 cm-1 correspond to the symmetric and asymmetric stretching of the COC group. The crystalline phase is associated with bands at 1274 and 1226 cm^{-1}, and the amorphous phase is associated with bands at 1261 and 1180 cm^{-1}. In the spectrum, it is possible to identify bands at 1700–1650 cm^{-1}, which are due to carbonyl stretching vibrations of ester groups of the polymer [28–32].

The spectra of pure PHB and films containing niobium oxyhydroxide have a similar band pattern. The band with a maximum at 1720 cm^{-1} is commonly exploited in the study of intramolecular and intermolecular interactions involving carbonyl groups because they are important in the organization of PHB crystals [33]. To obtain information on specific interactions in the polymer in the presence of inorganic particles, deconvolution of the bands in the carbonyl group region of the PHB was performed. This study was conducted using the Lorentzian function and is shown in Fig. 4. The fitting reveals the presence of three major bands located in the region between 1800 and 1640 cm-1 corresponding to the carbonyl groups of the crystalline and amorphous phases. The shoulder at 1740 cm-1 is associated with the free C═O, and the most intense band at 1722 cm^{-1} is associated with the C═O groups attached in both the crystalline and amorphous phases. The weak absorption band observed at 1686 cm^{-1} region can be assigned to C═O groups involved in interactions associated with the crystalline phase [34,35]. The 1–5 wt% PHB/S2 films did not show significant shifts in the bands at 1722 cm^{-1} and 1740 cm^{-1}. Comparing the PHB/S2 and pure PHB, is possible to identify only a smooth enlargement of these bands in the presence of the niobium compound. However, in the region of 1686 cm-1 significant shifts are observed when the concentration of the niobium compound increases in the polymer. According to Sato et al. [36] this low intensity band is important because it is sensitive to changes in the polymer structure, particularly the crystalline defects caused by chemical interactions among the components of blends and composites.

Films containing 3 and 5 wt% of niobium oxyhydroxide (PHB/S2_3 and PHB/S2_5) showed a shift of the band from 1687 cm-1 to 1676 cm-1 and 1674, respectively. From the similar behavior of the FTIR spectra reported in the literature, Díez-Pascual and Díez-Vicente [37] and Yu et al. [38] suggest that the interaction of PHB with niobium particles occurs by means of hydrogen bonds involving C═O groups from the ester groups of the PHB and —OH groups present in the niobium oxyhydroxide. The oxyhydroxide synthesized niobium was subjected to treatment with hydrogen peroxide as discussed by Oliveira et al. [39] and Esteves et al. [40] generating peroxo groups, which are highly oxidizing, and hydroxy groups on its surface.

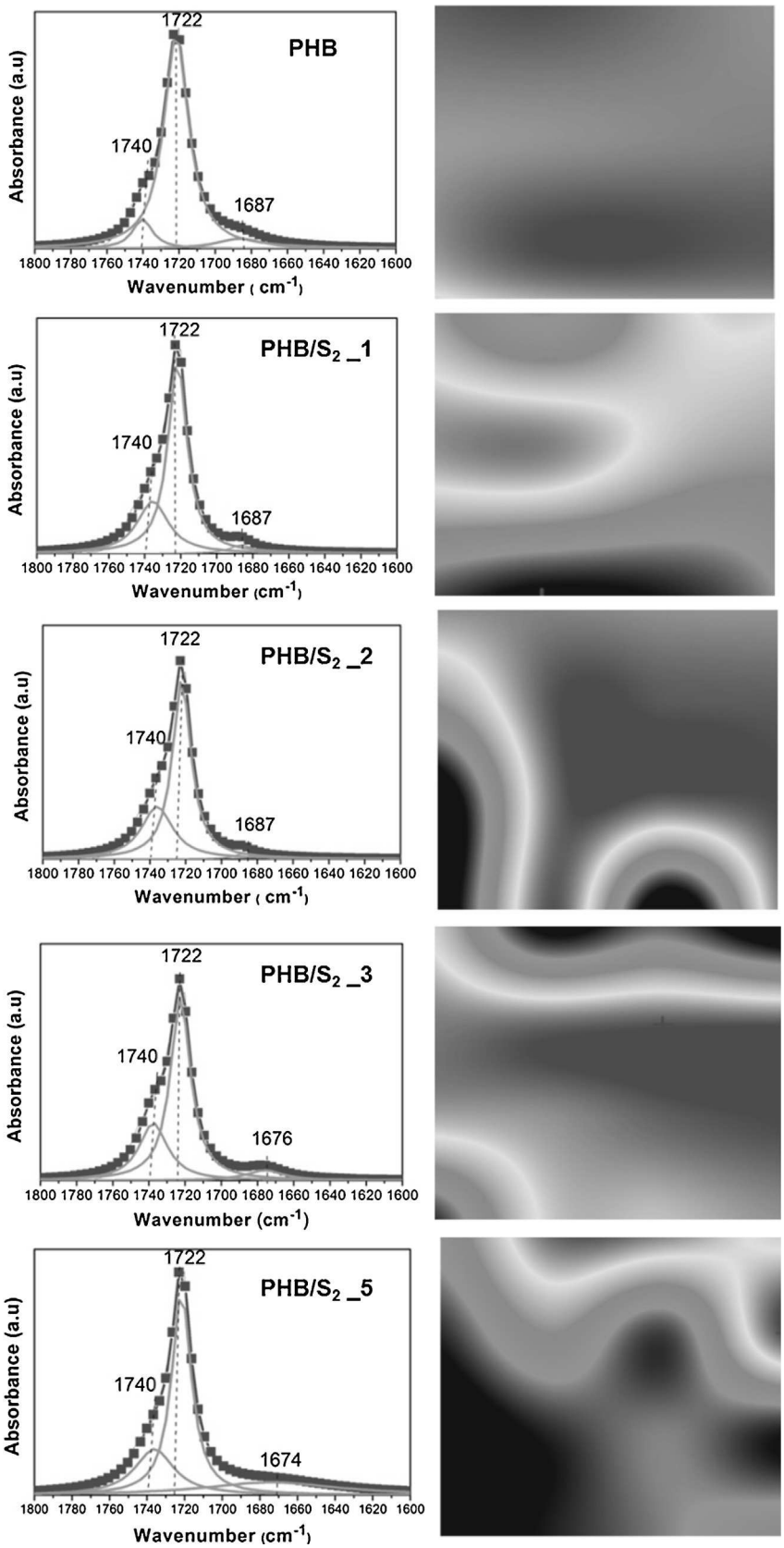

Fig. 4. Lorentzian fit for FTIR-ATR and characteristic curve contour profiles of the carbonyl regions of films of PHB and 1–5 wt% PHB/S2.

The images on the right side of the FTIR spectra in Fig. 4 correspond to the contour profiles of the band displayed in the region between 1800 and 1600 cm^{-1}. For PHB films, there was a single color in the image, showing that the profile of the band did not substantially change along the length of the sample scan. For samples containing PHB and particles of niobium, there is a different behav-

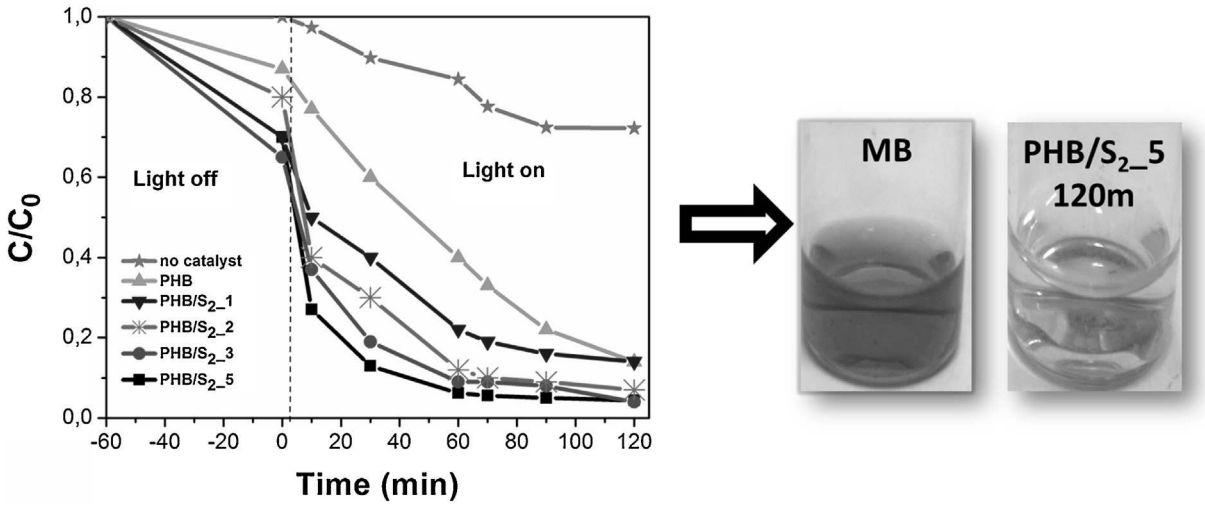

Fig. 5. A profile of the color removal kinetics of a methylene blue dye solution (20 mg L^{-1}) employing the PHB/S2 catalysts.

ior with a strong pattern of changing colors along the length of the sample during scanning to the extent that the concentration of niobium in the film phase increases. The interaction of C=O groups of the polymer with the niobium particles, which are dispersed in the matrix, most likely influenced the band profile, modifying it while scanning. It is believed that as the contribution of the vibrations of groups involved in interactions that occur in the regions of nanoparticle-polymer interface in the absorption band becomes higher, the appearance of other colors is observed.

3.2. Catalytic tests

3.2.1. Photocatalytic tests in the presence of UV radiation

The photodegradation of an aqueous solution of methylene blue in the presence of oxyhydroxide and PHB/niobium composite was monitored by UV–vis spectrometry, and the results are shown in Fig. 5.

When the pure PHB was employed, a low removal capacity by adsorption of the dye was observed, as shown in the profile of Fig. 5 in the absence of light. On the other hand, materials containing niobium oxyhydroxide had better adsorption capacities, and the PHB_5 catalyst showed a removal of approximately 30%. The curve shows that decoloration of the solution occurred only in the presence of UV light without catalytic, about 30% after 90 min (photolysis). In the presence of catalyst and UV light, the color removal of the dye solution was complete after 120 min. After the addition of pure PHB under UV light, the discoloration increased, this indicated that another process runs in addition to the photolysis. Probably this process is related to the formation of hydroxyl radicals, which are generally formed from the surface degradation of PHB in the presence of oxygen, humidity and UV radiation [41].

The composites that have oxyhydroxide niobium in their constitution revealed high catalytic activities compared to pure polymer. In fact, the materials containing 3–5 wt% of niobium oxyhydroxide showed complete removal of color after only 30 min of reaction time. The semiconductor niobium oxyhydroxide has a bandgap of 3.0 eV, as discussed earlier, which displays a good catalytic activity. Nogueira et al. [42] reported similar results using only the niobium oxyhydroxide after treatment with hydrogen peroxide. However, the use of finely powdered material without deposition over a polymeric matrix did not allow its recovery for reuse. Furthermore, the PHB/S2 composite showed a higher catalytic efficiency than SnO2 thin films which bandgap (3.6 eV) is higher than of niobium oxyhydroxide (3.0 eV) [40] and higher than nanotube titanium dioxide, a widely studied material for photocatalysis that showed 79% removal of methylene blue in an aqueous medium using UV radiation [43].

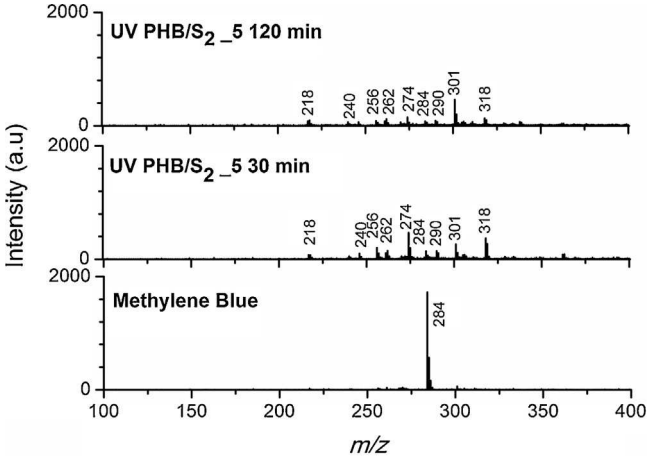

Fig. 6. ESI(+)-MS methylene blue solution before and after 30 and 120 min of reaction time using photocatalysis with the PHB/S2_5 catalyst under UV radiation.

While the materials presented in this work have shown high dye removal capacities, the study via UV–vis spectroscopy proves the effective degradation of the organic molecule. Thus, the degradation of methylene blue by niobium catalysts incorporated into PHB was monitored by ESI(+)-MS to identify photocatalysis intermediates (Fig. 6). The study was conducted after 30 and 120 min of reaction time. Due to its higher removal efficiency, the resulting reaction solution using the PHB/S_2_5 material was studied. The spectrum of the dye indicates the presence of a single peak at $m/z = 284$ that is characteristic of the methylene blue aqueous solution [44].

After reaction, the characteristic peak intensity of the dye decreases significantly, and other peaks associated with the intermediaries appear. Concurrently with the decrease of the $m/z = 284$ signal, there is the emergence of various ions ($m/z = 301$, 318, 338, 218, 262 and 256), suggesting the occurrence of the oxidation and demethylation reactions of dye molecules [43]. The peaks at $m/z = 256$ and $m/z = 274$ refer to the beginning of the degradation of the organic molecule indicating the demethylation of methylene blue. The signals $m/z = 218$, 240 and other signals with a lower mass than methylene blue are evidence that the structure of the molecule was degraded, which shows an advanced stage of oxidation before

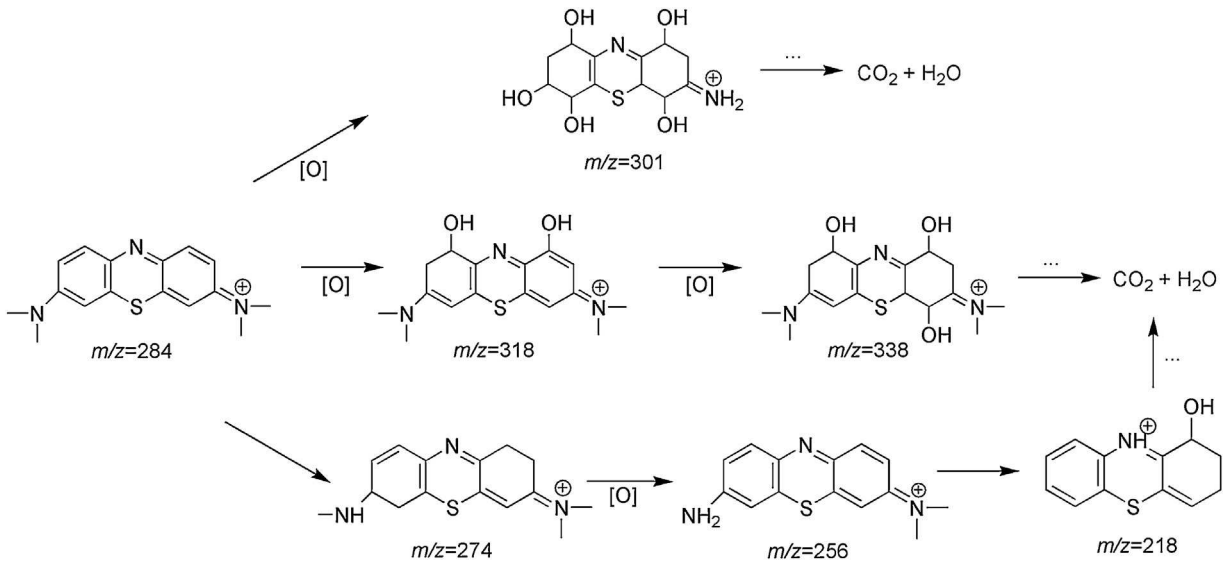

Fig. 7. Proposal of the main intermediaries involved in the degradation of methylene blue.

mineralization [45]. Furthermore, the signals at $m/z = 301$, $m/z = 318$ and $m/z = 338$ suggest successive hydroxylations, indicating that the HO• radicals generated *in situ* by the photocatalytic process are incorporated into the dye structure promoting its oxidation [27,46,47]. It is interesting to note that with only 30 min of reaction time, it is possible to identify a large proportion of ions corresponding to significant dye degradation with a decreasing signal at a $m/z = 284$ concerning the dye. The spectrum of the solution obtained after 120 min of reaction shows the signals referring to the same intermediates but with less intensity, indicating that there was degradation of these compounds, possibly via mineralization. The occurrence of other peaks associated with intermediate species after the reaction shows that the degradation of the dye occurs instead of only the adsorption process.

The structures of the intermediates are proposed in Fig. 7.

Yew et al. [10] conducted a similar study to the one presented here, where a PHB polymer matrix was employed for the dispersion of TiO_2 semiconductor. The authors succeeded in removing 96% of the methylene blue dye. However, higher catalyst concentrations were used in the polymer (57% TiO2) compared to in this work as well as a lower concentration of methylene blue. In addition, there was no evidence that the dye was in fact degraded because studies showed no evidence of reaction intermediates as presented via ESI–MS in this study.

The particles of niobium oxyhydroxide after treatment with hydrogen peroxide have been the subject of several studies of our research group, in which the high removal capacity of organic compounds in solution was demonstrated [48]. In the studies, it became apparent that the surface is formed from modified niobium forming "peroxo" groups, which are highly oxidizing. Such oxidizing species can be transferred to the organic compounds in solution, causing their effective oxidation [49]. Additionally, because it is a semiconductor, highly oxidizing hydroxyl radicals can be generated *in situ* by the action of visible or UV radiation. The matrix PHB, due to its hydrophobicity, showed a high stability in the aqueous medium in the presence of visible and UV radiation. With the immobilization of the catalyst to niobium in the polymer matrix, its removal from the aqueous medium has become easier, thus eliminating the costly filtration or centrifugation step and allowing it to be reused for several photocatalytic cycles. To evaluate the stability of the catalyst, the composite showing the best efficiency in the photocatalytic process, PHB/S2_5, was reused for seven successive cycles of 120 min as shown in Fig. 7. To evaluate the stability of the catalyst, the composite showing the best efficiency in the photocatalytic process, PHB/S2_5, was reused for seven successive cycles of 120 min, as shown in Fig. 8.

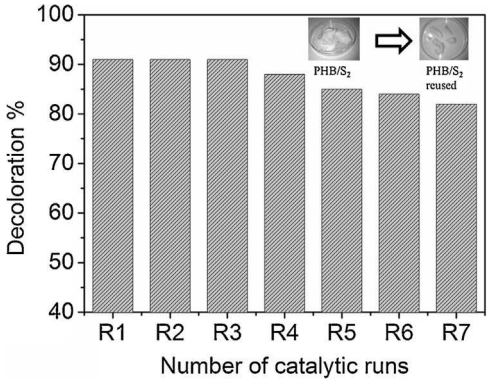

Fig. 8. Color removal of a methylene blue solution (20 mg L^{-1}) after successive reuse of a PHB/S2_5 catalyst.

The catalytic activity was maintained for seven reuses and showed a high removal efficiency of approximately 90% for all of the tests. After being reused, the modified films were a noticeably blue color, most likely due to the adsorption of methylene blue solution, which can be a cause of the partial loss of activity throughout the reuses. SEM images of the PHB/S2_5 catalyst (Fig. 9) after the seventh reuse show the presence of niobium oxyhydroxide, which is mainly present on the surface of PHB, justifying the maintenance of its activity after several reuses.

The EDS spectra obtained for the PHB/S2_5 material before the reaction (Fig. 3) and after seven reuse cycles (Fig. 9) are similar. Comparing the images of the surface and fracture of PHB/S2_5, it is observed that the niobium compound clusters are distributed throughout the material suggesting that there is the preferential accumulation of the niobium oxyhydroxide phase on the surface film and that there is no leaching of the active phase after successive reuses. Furthermore, the recovery of the niobium particles from the PHB matrix becomes possible by solubilization, making this polymer interesting as a substrate for photocatalysis and giving it a great advantage over other materials studied.

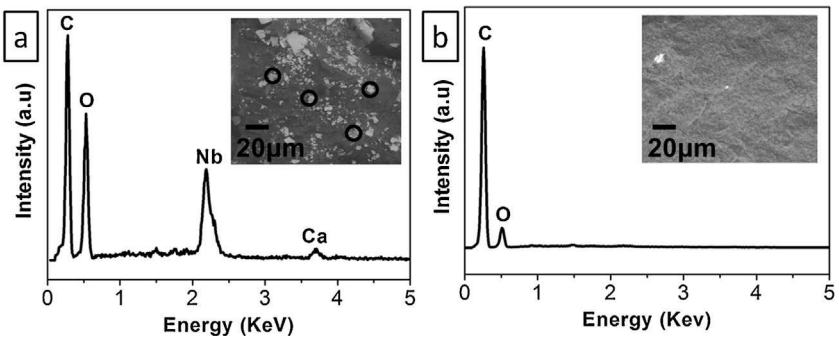

Fig. 9. SEM images/EDS of PHB/S2_5 after seven reuses: (a) surface and (b) fracture.

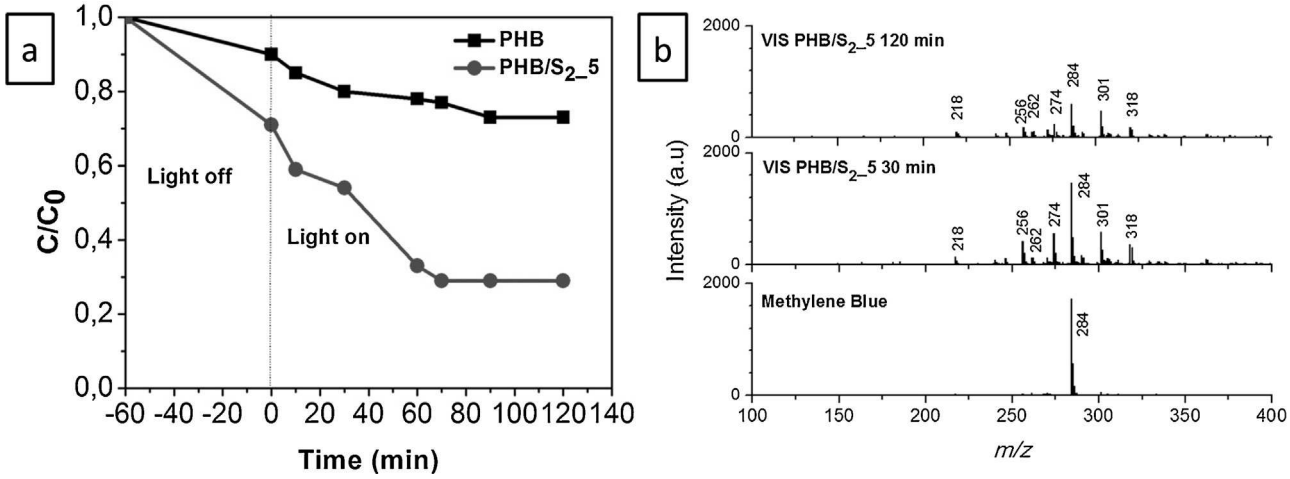

Fig. 10. Profile of methylene blue dye removal (20 mg L^{-1}) employing the pure PHB and PHB/S2_5 catalysts (a), and the ESI–MS signals of the intermediates after 30 and 120 min of reaction time (b).

3.2.2. Photocatalytic tests in the presence of UV–vis irradiation

The material with the best catalytic activity has been tested for the removal of methylene blue using photocatalysis under the action of visible light. This test can indicate the potential of the material to be applied using solar radiation, which would make the process less onerous in the case of use on an industrial scale. Fig. 10a shows the profile of the color removal kinetics comparing the pure PHB and PHB/S2_5 catalysts. The pure PHB showed the ability to remove approximately 25% of the dye from the aqueous medium. The presence of niobium oxyhydroxide in the polymer matrix of the dye significantly improves the removal capacity, removing approximately 70% of the coloring. Again, this process was studied through the formation of intermediates by ESI–MS (Fig. 10b).

After 30 min of reaction time, peaks relating to successive hydroxylations of the dye molecule were observed, indicating the action of $OH^{\bullet}$ radicals from the photocatalytic process. After 120 min of reaction time, the signal $m/z = 284$ referring to the dye decreases sharply with increasing intensities of signals relating to reaction intermediates. This result indicates that visible light can generate electron-hole pairs promoting the generation of the hydroxyl radical, which is capable of oxidizing organic molecules. The catalytic effect of the presence of visible light is less effective when compared to UV light, but the use of sunlight has been shown to be quite promising.

3.2.3. Photocatalytic tests in continuous flow

A continuous flow test has been conducted to obtain an applied photocatalytic system for the degradation of methylene blue molecules using UV radiation. The measurement of the color removal was obtained continuously every 10 min of reaction time with a UV–vis spectrometer using the determined wavelength of 664 cm^{-1}.The efficiency of the photocatalysis is shown in Fig. 11.

In the flow reactor, methylene blue decoloration in the absence of catalyst under UV radiation was not significant. When the catalyst system employed PHB/S2_5, maximum removal due to photocatalysis remained approximately 90%, similar to the decoloration batch process, whose removal rate reached 96%. The decoloration balance of the photocatalytic process was reached after 300 min. The formation of intermediates was studied by ESI–MS after 530 min of reaction time, and the results are shown in Fig. 11. The intermediates formed during a reaction indicated that the bleaching process should occur effectively by means of photocatalysis. In the continuous flow system, the mechanism has been identified largely from intermediates that are also present in the batch process suggesting that the photocatalysis occurs by the same proposed mechanism forming the structures depicted in Fig. 7.

Mathews [50] used a borosilicate continuous flow system coated with sand impregnated with TiO2, and a 70% removal of methylene blue in the presence of UV radiation was observed. Recently, McCullagh et al. [51] reported the complete degradation of methylene blue using 90–120 g of TiO2 pellets as a catalyst, and Han et al. [52] used glass substrate covered with ZnO nanowires and UV radiation to reach a maximum methylene blue removal of 96%.

This study proposes a system for continuous flow whose polymer film containing the catalyst can be easily removed from the aqueous medium and reused. It is not necessary to use separation methods such as centrifugation or hydrocyclone to separate the catalyst from the aqueous medium making it difficult to reuse as was seen in the studies. Furthermore, the amount of catalyst used is greatly reduced. The efficient polymer/catalyst photocat-

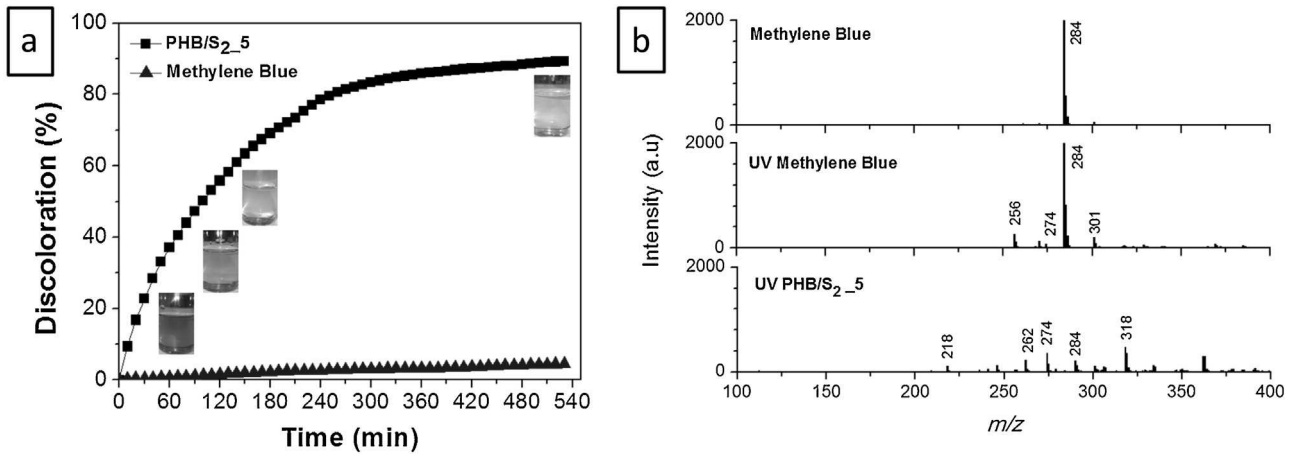

Fig. 11. A profile of the color removal kinetics of a methylene blue dye solution (20 mg L^{-1}) employing the PHB/S2_5 catalyst in continuous flow (a), and the ESI–MS signals of the intermediate after 530 min of reaction time (b).

alytic system presents with a potential application in the treatment of colored industrial wastewater.

4. Conclusions

In this work, a catalyst based on dispersed niobium oxyhydroxide in a biodegradable polymeric matrix (PHB) was developed for the first time. The formed composite proved to be highly efficient for the removal of an organic dye from the aqueous medium in the presence of UV or visible radiation via photocatalysis. SEM analysis suggests that the particles of niobium oxyhydroxide are finely agglomerated and highly distributed throughout the bulk PHB.

The PHB film modified with catalyst remained stable, indicating a slight decrease in color removal after being reused for seven cycles. The photocatalytic tests in continuous flow showed a high catalytic activity using the compound PHB/S2, which was easily recovered from the aqueous solution after the photocatalysis steps without requiring filtration or centrifugation. Finally, the ESI–MS study showed an enhanced dye oxidation stage, indicating that in fact the degradation of the organic dye occurs.

Acknowledgments

This work was supported by grants from CNPq, FAPEMIG and CAPES.

Appendix A. Supplementary data

Supplementary data associated with this article can be found, in the online version, at http://dx.doi.org/10.1016/j.apcatb.2016.02.031.

References

[1] I.K. Konstantinou, T.A. Albanis, Appl. Catal. B Environ. 49 (2004) 1–14.
[2] M.M. Khin, A.S. Nair, V.J. Babu, R. Murugan, S. Ramakrishna, Energy Environ. Sci. 5 (2012) 8075–8109.
[3] P. Chagas, H.S. Oliveira, R. Mambrini, M. Le Hyaric, M.V. De Almeida, L.C.A. Oliveira, Appl. Catal. A Gen. 454 (2013) 88–92.
[4] Z. Liu, Y.E. Miao, M. Liu, Q. Ding, W.W. Tjiu, X. Cui, T. Liu, J. Colloid Interface Sci. 424 (2014) 49–55.
[5] J.D. Torres, E. a. Faria, J.R. SouzaDe, A.G.S. Prado, J. Photochem. Photobiol. A Chem. 182 (2006) 202–206.
[6] O.F. Lopes, E.C. Paris, C. Ribeiro, Appl. Catal. B Environ. 144 (2014) 800–808.
[7] M. Zarei-Chaleshtori, M. Hosseini, R. Edalatpour, S.M.S. Masud, R.R. Chianelli, Microchem. J. 110 (2013) 361–368.
[8] L.C.A. Oliveira, M. Gonçalves, M.C. Guerreiro, T.C. Ramalho, J.D. Fabris, M.C. Pereira, K. Sapag, Appl. Catal. A Gen. 316 (2007) 117–124.
[9] J.C. Rooke, T. Barakat, J. Brunet, Y. Li, M.F. Finol, J.F. Lamonier, J.M. Giraudon, R. Cousin, S. Siffert, B.L. Su, Appl. Catal. B Environ. 162 (2015) 300–309.
[10] S.P. Yew, H.Y. Tang, K. Sudesh, Polym. Degrad. Stab. 91 (2006) 1800–1807.
[11] G.F. Shan, X. Gong, W.P. Chen, L. Chen, M.F. Zhu, Colloid Polym. Sci. 289 (2011) 1005–1014.
[12] J.H. Yang, Y.S. Han, J.H. Choy, Thin Solid Films 495 (2006) 266–271.
[13] A.H. Fostier, M.D.S.S. Pereira, S. Rath, J.R. Guimarães, Chemosphere 72 (2008) 319–324.
[14] F. Wang, S.X. Min, Chinese Chem. Lett. 18 (2007) 1273–1277.
[15] S. Ghosh, N.A. Kouamé, L. Ramos, S. Remita, A. Dazzi, A. Deniset-Besseau, P. Beaunier, F. Goubard, P.H. Aubert, H. Remita, Nat. Mater. (2015) 1–7.
[16] A. Mohamed El-Hadi, Polym. Bull. 71 (2014) 1449–1470.
[17] G. Burlein, M. Rocha, Mater. Res. 17 (2014) 203–212.
[18] M.P. Arrieta, E. Fortunati, F. Dominici, E. Rayón, J. López, J.M. Kenny, Polym. Degrad. Stab. 107 (2014) 139–149.
[19] A. Sathish, K. Glaittli, R.C. Sims, C.D. Miller, J. Polym. Environ. 22 (2014) 272–277.
[20] M.J. Fabra, A. Lopez-Rubio, J.M. Lagaron, J. Food Eng. 127 (2014) 1–9.
[21] M. Naffakh, C. Marco, G. Ellis, S.R. Cohen, A. Laikhtman, L. Rapoport, A. Zak, Mater. Chem. Phys. 147 (2014) 273–284.
[22] A. Murphy, Sol. Energy Mater. Sol. Cells. 91 (2007) 1326–1337.
[23] X. Li, D. Wang, G. Cheng, Q. Luo, J. An, Y. Wang, Appl. Catal. B Environ. 81 (2008) 267–273.
[24] P.S.D.O. Patrício, F.V. Pereira, M.C. Dos Santos, P.P. De Souza, J.P.B. Roa, R.L. Orefice, J. Appl. Polym. Sci. 127 (2013) 3613–3621.
[25] L.C.A. Oliveira, M.F. Portilho, A.C. Silva, H.A. Taroco, P.P. Souza, Appl. Catal. B Environ. 117-118 (2012) 29–35.
[26] R.M. Cornell, U. Schwertmann, The Iron Oxides, 2nd. ed., J. Willey-VCH, New York, 2003.
[27] L.C.A. de Oliveira, N.T. Costa, J.R. Pliego, A.C. Silva, P.P. de Souza, P.S. Patrícia, Appl. Catal. B Environ. 147 (2014) 43–48.
[28] A. Salehabadi, M.A. Bakar, N.H.H.A. Bakar, Materials (Basel) 7 (2014) 4508–4523.
[29] C.P. Liau, M. Bin Ahmad, K. Shameli, W. Zin, W. Yunus, N.A. Ibrahim, N. Zainuddin, Y.Y. Then, Sci. World J. 2014 (2014) 1–9.
[30] H.S. Barud, J.L. Souza, D.B. Santos, M.S. Crespi, C.A. Ribeiro, Y. Messaddeq, S.J.L. Ribeiro, Carbohydr. Polym. 83 (2011) 1279–1284.
[31] Y.T. Ong, A.L. Ahmad, S.H.S. Zein, K. Sudesh, S.H. Tan, Sep. Purif. Technol. 76 (2011) 419–427.
[32] G.R. Saad, H.E. Salama, N.A. Mohamed, M.W. Sabaa, J. Appl. Polym. Sci. 131 (2014) 9395–9407.
[33] J.P.B. Roa, P.S.D.O. Patrício, R.L. Oréfice, R.M. Lago, J. Appl. Polym. Sci. 128 (2013) 3019–3025.
[34] T. Furukawa, H. Sato, R. Murakami, J. Zhang, Y.X. Duan, I. Noda, S. Ochiai, Y. Ozaki, Macromolecules 38 (2005) 6445–6454.
[35] H. Sato, Y. Ando, J. Dybal, T. Iwata, I. Noda, Y. Ozaki, Macromolecules 41 (2008) 4305–4312.
[36] H. Sato, R. Murakami, A. Padermshoke, Macromolecules 37 (2004) 7203–7213.
[37] A.M. Díez-Pascual, A.L. Díez-Vicente, Int. J. Mol. Sci. 15 (2014) 10950–10973.
[38] Q. Yu, J. Xu, J. Liu, B. Li, Y. Liu, Y. Han, Appl. Surf. Sci. 263 (2012) 532–535.
[39] L.C.A. Oliveira, H.S. Oliveira, G. Mayrink, H.S. Mansur, A.A.P. Mansur, R.L. Moreira, Appl. Catal. B Environ. 152–153 (2014) 403–412.
[40] A. Esteves, L.C.A. Oliveira, T.C. Ramalho, M. Goncalves, A.S. Anastacio, H.W.P. Carvalho, Catal. Commun. 10 (2008) 330–332.
[41] B. Singh, N. Sharma, Polym. Degrad. Stab. 93 (2008) 561–584.
[42] A.E. Nogueira, T.C. Ramalho, L.C.A. Oliveira, Top. Catal. 54 (2011) 270–276.
[43] J. Khan, S.E. Harton, P. Akcora, B.C. Benicewicz, S.K. Kumar, Macromolecules 42 (2009) 5741–5744.

[44] I.S.X. Pinto, P.H.V.V. Pacheco, J.V. Coelho, E. Lorençon, J.D. Ardisson, J.D. Fabris, P.P. Souza, K.W.H. Krambrock, L.C.A. Oliveira, M.C. Pereira, Appl. Catal. B Environ. 119–120 (2012) 175–182.
[45] C.S. Castro, M.C. Guerreiro, L.C.A. Oliveira, M. Gonçalves, A.S. Anastácio, M. Nazzarro, Appl. Catal. A Gen. 367 (2009) 53–58.
[46] W.F. de Souza, I.R. Guimarães, M.C. Guerreiro, L.C.A. Oliveira, Appl. Catal. A Gen. 360 (2009) 205–209.
[47] M.C. Pereira, F.S. Coelho, C.C. Nascentes, J.D. Fabris, M.H. Araújo, K. Sapag, L.C.A. Oliveira, R.M. Lago, Chemosphere 81 (2010) 7–12.
[48] A.C. Silva, R.M. Cepera, M.C. Pereira, D.Q. Lima, J.D. Fabris, L.C.A. Oliveira, Appl. Catal. B Environ. 107 (2011) 237–244.
[49] H.S. Oliveira, L.D. Almeida, V.A.A. De Freitas, F.C.C. Moura, P.P. Souza, L.C.A. Oliveira, Catal. Today 240 (2015) 176–181.
[50] R.W. Matthews, Water Res. 25 (1991) 1169–1176.
[51] C. McCullagh, P.K.J. Robertson, M. Adams, P.M. Pollard, A. Mohammed, J. Photochem. Photobiol. A Chem. 211 (2010) 42–46.
[52] Z. Han, J. Li, W. He, S. Li, Z. Li, J. Chu, Y. Chen, Microelectron. Eng. 111 (2013) 199–203.